Developmental Biology 409 (2016) 55–71

Contents lists available at ScienceDirect

Developmental Biology

journal homepage: www.elsevier.com/locate/developmentalbiology

Primary cilia are critical for Sonic hedgehog-mediated dopaminergic neurogenesis in the embryonic midbrain

Mary Gazea [a,1,2], Evangelia Tasouri [b,c,1], Marianna Tolve [a], Viktoria Bosch [a], Anna Kabanova [a], Christian Gojak [d,e,3], Bahtiyar Kurtulmus [f], Orna Novikov [g], Joachim Spatz [d,e], Gislene Pereira [f], Wolfgang Hübner [h], Claude Brodski [g], Kerry L. Tucker [b,c,i,*], Sandra Blaess [a,**]

[a] Institute of Reconstructive Neurobiology, University of Bonn, 53127 Bonn, Germany
[b] Interdisciplinary Center for Neurosciences, University of Heidelberg, 69120 Heidelberg, Germany
[c] Institute of Anatomy and Cell Biology, University of Heidelberg, 69120 Heidelberg, Germany
[d] Department of Biophysical Chemistry, University of Heidelberg, 69120 Heidelberg, Germany
[e] Department of New Materials and Biosystems, Max Planck Institute for Intelligent Systems, 70569 Stuttgart, Germany
[f] Molecular Biology of Centrosomes and Cilia, German Cancer Research Center, DKFZ-ZMBH Alliance, 69120 Heidelberg, Germany
[g] Department of Physiology and Cell Biology, Zlotowski Center for Neuroscience, Faculty of Health Sciences, Ben-Gurion University of the Negev, Beer Sheva 84105, Israel
[h] Molecular Biophotonics, University of Bielefeld, 33615 Bielefeld, Germany
[i] University of New England, College of Osteopathic Medicine, Department of Biomedical Sciences, Center for Excellence in the Neurosciences, Biddeford, ME 04005, USA

ARTICLE INFO

Article history:
Received 15 February 2015
Received in revised form
21 October 2015
Accepted 30 October 2015
Available online 2 November 2015

Keywords:
Primary cilia
Ift88
Intraflagellar transport
Midbrain
Dopaminergic neurons
Shh

ABSTRACT

Midbrain dopaminergic (mDA) neurons modulate various motor and cognitive functions, and their dysfunction or degeneration has been implicated in several psychiatric diseases. Both Sonic Hedgehog (Shh) and Wnt signaling pathways have been shown to be essential for normal development of mDA neurons. Primary cilia are critical for the development of a number of structures in the brain by serving as a hub for essential developmental signaling cascades, but their role in the generation of mDA neurons has not been examined. We analyzed mutant mouse lines deficient in the intraflagellar transport protein IFT88, which is critical for primary cilia function. Conditional inactivation of *Ift88* in the midbrain after E9.0 results in progressive loss of primary cilia, a decreased size of the mDA progenitor domain, and a reduction in mDA neurons. We identified Shh signaling as the primary cause of these defects, since conditional inactivation of the Shh signaling pathway after E9.0, through genetic ablation of *Gli2* and *Gli3* in the midbrain, results in a phenotype basically identical to the one seen in *Ift88* conditional mutants. Moreover, the expansion of the mDA progenitor domain observed when Shh signaling is constitutively activated does not occur in absence of *Ift88*. In contrast, clusters of Shh-responding progenitors are maintained in the ventral midbrain of the hypomorphic *Ift88* mouse mutant, *cobblestone*. Despite the residual Shh signaling, the integrity of the mDA progenitor domain is severely disturbed, and consequently very few mDA neurons are generated in *cobblestone* mutants. Our results identify for the first time a crucial role of primary cilia in the induction of mDA progenitors, define a narrow time window in which Shh-mediated signaling is dependent upon normal primary cilia function for this purpose, and suggest that later Wnt signaling-dependent events act independently of primary cilia.

* Correspondence to: University of New England, College of Osteopathic Medicine, Department of Biomedical Sciences, Center for Excellence in the Neurosciences, 11 Hills Beach Rd., Biddeford, ME 04005, USA. Fax: +1 207 202 5887.
** Correspondence to: University of Bonn, Institute of Reconstructive Neurobiology, Sigmund-Freud-Str. 25, 53127 Bonn, Germany. Fax: +49 6885 501.
E-mail addresses: ktucker2@une.edu (K.L. Tucker), sblaess@uni-bonn.de (S. Blaess).
[1] Equal contribution.
[2] Current adress: Max Planck Institute of Psychiatry, Kraepelinstraße 2-10, 80804 Munich, Germany.
[3] Current address: PromoCell GmbH, Sickingerstr. 63/65, 69126 Heidelberg, Germany.

http://dx.doi.org/10.1016/j.ydbio.2015.10.033
0012-1606/

1. Introduction

Midbrain dopaminergic (mDA) neurons regulate movement, reward behavior, and cognitive function, and their degeneration or dysfunction is implicated in a number of neurological diseases, including Parkinson's disease, schizophrenia, and depression (Albin et al., 1989; Tye et al., 2013; Winterer and Weinberger, 2004). The anatomy and physiology of mDA neurons have been studied extensively, but the mechanisms underlying their development are still not understood. Recent studies conclusively showed that mDA neurons arise from neural progenitors in the ventral midline (floor plate) of the embryonic midbrain (reviewed in (Blaess and Ang, 2015)). These mDA progenitors are defined by the expression of the transcription factors Lmx1a/b (LIM homeobox transcription factor 1 alpha/beta) and Foxa1/2 (forkhead box 1/2), and the secreted morphogen Shh (Sonic Hedgehog) (Andersson et al., 2006; Deng et al., 2011; Lin et al., 2009; Nakatani et al., 2010; Yan et al., 2011). The induction of these factors in the floor plate and subsequent induction of mDA progenitors is dependent on signaling pathways activated by Shh, Wnts, and fibroblast growth factors (Fgf) (Andersson et al., 2006; Andersson et al., 2013; Blaess et al., 2006; Farkas et al., 2003; Fernando et al., 2014; Lahti et al., 2012; Yang et al., 2013; Ye et al., 1998).

Shh is critical for specification of ventral cell fates in many parts of the nervous system. Shh signaling is transduced by the transmembrane receptors patched (Ptch) and Smoothened (Smo) and intracellularly by the Gli zinc-finger transcription factors (Gli1-3). Gli2 is the main activator downstream of Shh signaling; Gli3 acts as a repressor in the pathway (Fuccillo et al., 2006). The formation of both a Gli2 transcriptional activator and a Gli3 transcriptional repressor – and consequently Hedgehog signaling – is critically dependent upon a functional primary cilium in the responding cell (Goetz and Anderson, 2010). Primary cilia are short protrusions from the plasma membrane that are found extending from the surface of most vertebrate cell types (Hoyer-Fender, 2013). The axonemal center of the cilium is composed of ordered microtubule doublets originating in a centrosome-derived basal body. Trafficking of cargo, including signal transduction proteins, into and out of the cilium is a tightly-regulated process dependent upon intraflagellar transport (IFT). IFT utilizes the motor proteins kinesin-II and cytoplasmic dynein-II for anterograde and retrograde transport, respectively, while proteins of the IFT-B and IFT-A classes, respectively, are critical for both transport and signal transduction (Scholey, 2003). Genetic evidence has revealed that multiple mutants in IFT proteins, and in proteins localized to the basal body or the axoneme, demonstrate characteristic defects in Shh signaling in organs throughout the body (Tasouri and Tucker, 2011). Cell biological analysis has shown that crucial components of Hedgehog signaling specifically localize to the cilia in a dynamic fashion, including Ptch1, Smo, and the Gli proteins (Corbit et al., 2005; Haycraft et al., 2005; Rohatgi et al., 2007).

In addition, both canonical and non-canonical Wnt signaling pathways have also been implicated in the functional biology of primary cilia, but the evidence for their absolute dependence upon primary cilia function is controversial. Studies in different organ systems such as the forebrain, skeleton, and abdominal viscera, indicate that the disruption of cilia- or basal body-localized proteins results in dysfunctional Wnt signaling (in terms of beta-catenin or Axin2 levels as a readout for canonical signaling, or defects in convergent extension movements during gastrulation) (Oh and Katsanis, 2012). However, comprehensive studies examining early development in zebrafish and mice lacking primary cilia observed no defects in classic Wnt-dependent developmental processes (Huang and Schier, 2009; Ocbina et al., 2009; Tran et al., 2008). Clearly, abnormalities in Wnt signaling are also observed in progression to cystic kidney disease when proteins localizing to cilia and basal bodies bear mutations (Lienkamp et al., 2012). To reconcile these disparate findings, various possibilities exist, including the idea that Wnt signaling is dependent upon basal body function, but not on IFT or axoneme-localized ciliary processes (Huang and Schier, 2009). Alternatively, subcellular localization of "ciliary" proteins distinct from the primary cilium / basal body may be responsible for modifications in Wnt signaling pathways.

Given that both Shh and Wnt signaling are essential for the specification of mDA progenitors, and that not only Shh, but also Wnt signaling may depend upon primary cilia function, it is of great interest to understand the impact of primary cilia function on mDA specification. Here we address this question using mouse genetic models in which IFT and Shh signaling components are disrupted.

2. Materials and methods

2.1. Mouse lines

All experiments were conducted according to the guidelines of the states of Baden-Württemberg and North Rhine-Westphalia, Germany. *cbbs* (Willaredt et al., 2008), $Ift88^{flox}$ (Haycraft et al., 2007), $Gli3^{Xt}$ (Hui and Joyner, 1993), $Gli2^{zfd}$ (Matise et al., 1998), $Gli2^{flox}$ (Corrales et al., 2006), $Gli3^{flox}$ (Blaess et al., 2008), $R26^{SmoM2}$ (Jeong et al., 2004), and $En1^{Cre}$ (Kimmel et al., 2000) alleles were generated as described. 12 noon of the day of the vaginal plug was assigned the date embryonic day 0.5 (E0.5). To generate conditional knockout (cko) mice or mice in which the Shh signaling receptor Smo was conditionally activated (ca), $En1^{Cre/+}$ mice were crossed with mice bearing floxed alleles (genotypes in brackets): *Ift88*-cko ($En1^{Cre/+}$, $Ift88^{flox/flox}$), *Gli2/3*-cko ($En1^{Cre/+}$, $Gli2^{flox/zfd}$, $Gli3^{flox/xt}$), Smo-ca ($En1^{Cre/+}$, $SmoM2^{flox/+}$) and *Ift88*-cko; Smo-ca ($En1^{Cre/+}$, $Ift88^{flox/flox}$, $SmoM2^{flox/+}$). For all embryonic stages before E12.5, somite-matched embryos were compared for analysis as follows: E9.5: 21-29 somites, E10.5: 35-39 somites; E11.5: >45 somites (Theiler, 1989). Genomic DNA was isolated from embryonic and adult tissue as described (Laird et al., 1991). For PCR genotyping the following primers were utilized Cre-F: 5′-TAAAGATATCTCACGTACTGACGGTG-3′, Cre-R: 5′-TCTCTGACCAGAGTCATCETTAGC-3′, En1WT-F: 5′-CACCGCACCACCAACTTTTTC-3′, En1WT-R: 5′-TCGCATCTGGAGCACACAAGAG-3′, Gli3 P1: 5′-GGCCCAAACATCTACCAACACATAG-3′, Gli3 P2: 5′-GTTGGCTGCTGCATGAAGACTGAC-3′, Gli3 P3: 5′-TACCCCAGCAGGAGACTCAGATTAG-3′, Gli3 P4: 5′-AAACCCGTGGCTCAGGACAAG-3′, Gli2-S: 5′-AAACAAAGCTCCTGTACACG-3′, Gli2-AS: 5′-CACCCCAAAGCATGTGTTTT-3′, Gli2neo-PA: 5′-ATGCCTGCTCTTTACTGAAG-3′, Gli2flox-C: 5′-AGGTCCTCTTATTGTCAAG-3′, Gli2flox-D: 5′-GAGACTCCAAGGTACTTAGC-3′, Ift88 common 5′ primer: 5′-GCCTCCTGTTTCTTGACAACA GTG-3′, Ift88 3′ flox and WT allele primer: 5′-GGTCCTAACAAGTAAGCCCAGTGTT-3, R26SMO: R26SMO YFP_F: 5′-CCT CGT GAC CAC CTT CG-3′, R26SMO YFP_R: 5′-TTG ATG CCG TTC TTC TGC-3′.

2.2. Immunohistochemical analysis

Embryos or embryonic brains were dissected, collected in cold 0.1 M phosphate-buffered saline (PBS), and embryonic tail samples were collected separately for DNA extraction and genotyping. The embryos were fixed for periods of 30 min to overnight at 4 °C in 4% paraformaldehyde (PFA) in 0.1 M PBS. After rinsing twice in 0.1 M PBS for 30 min the embryos were either treated in an ascending sucrose series (10, 20, and 30% in 0.1 M PBS) and mounted in Jung tissue freezing medium (Leica Biosystems, Wetzlar, Germany) or dehydrated and processed for paraffin embedding. Stainings of 10–14 μm cryosections or 7 μm paraffin sections were performed as described (Blaess et al., 2011; Brachmann et al., 2007) with the

following primary antibodies: anti-nestin (Rat-401 clone; EMD Millipore, Billerica, Massachusetts, USA) 1:1000; rabbit anti-BLBP (AB9558; EMD Millipore) 1:1000; mouse anti-γ-tubulin (clone GTU-88, Sigma-Aldrich) 1:1000; rabbit anti-Arl13b (kind gift of Tamara Caspary, Emory University, Atlanta, USA) 1:1500; guinea pig anti-Ift88 (ab42497, goat polyclonal, Abcam, Cambridge. UK) 1:500; rabbit or mouse anti-TH (AB152, MAB318, EMD Millipore) 1:500; rabbit anti-Lmx1a (AB10533; EMD Millipore) 1:1000; goat anti-FoxA2 (clone M-20; Santa Cruz Biotechnology) 1:1000, rat anti- DAT (AB369; EMD Millipore) 1:1000, rabbit anti- Nurr1 (sc-990; Santa Cruz Biotechnology) 1:250, rabbit anti-Pitx3 (38-2850; Thermo Fischer Scientific) 1:250 and mouse anti-Nkx6-1 (clone F55A10 developed by OD Madsen; Developmental Studies Hybridoma Bank) 1:50. The following secondary antibodies were used: Cy3-conjugated donkey anti-rabbit, anti-mouse or anti-goat (Cat.No. 11-165-152, 715-165-150 or 05-165-147, Jackson ImmunoResearch Laboratories, West Grove, USA) 1:200; Alexa 488-conjugated donkey anti-rabbit or anti-mouse IgG (Cat.No. AB150149, A21206 or A21202, Life Technologies, Carlsbad, USA) 1:500, Alexa 488-conjugated goat anti-rabbit, anti-mouse IgG or IgG1, Alexa 546-conjugated goat anti rabbit or anti-guinea pig (Cat.No., A11034, A11029, A21121, A11035, A11074, Life Technologies) 1:1000. For immunofluorescent detection of transcription factors, sections were treated with 1 mM EDTA at 65 °C for 10 min and incubated with biotinylated anti-mouse or anti-goat secondary antibodies (1:200, Cat.No. 715-065-150 or 711-065-152, Jackson Immuno Research) followed by Cy3-conjugated Streptavidin (Cat.No. 016-160-084, Jackson ImmunoResearch Laboratories, West Grove, USA) 1:1000.

2.3. Production of guinea pig and rabbit anti-Ift88 antibodies

Rabbit and guinea pig polyclonal antibodies were generated against carboxy terminal 459 amino acids of Ift88 fused to maltose binding protein (MBP-C-Ift88; kindly provided by GJ Pazour) (Pazour, 2002). Briefly, BL21DE3 cells expressing MBP-C-Ift88 were induced with 0.1 M IPTG at 30 °C for 3.5 h. Cells were lysed in 50 mM HEPES pH 7.0, 200 mM NaCl, 2 mM $MgCl_2$, 4 mM DTT, 1 mM benzamidine, 4 mM PMSF. The clarified cell extract was incubated with amylose resin (New England Biolabs, Frankfurt, Germany) for 2 h at 4 °C. MBP-C-Ift88 was eluted with 50 mM HEPES pH 7.0, 200 mM NaCl, 2 mM $MgCl_2$, 1 mM DTT, and 10 mM maltose. The purified MBP-C-Ift88 protein was injected in rabbits or guinea pigs using standard procedures (PSL GmbH, Heidelberg, Germany).

For affinity purification, glutathione S-transferase C-Ift88 (GST-C-Ift88; kindly provided by GJ Pazour) (Pazour, 2002) was induced in *Escherichia coli* as described above and purified using Glutathione Sepharose beads (GE Healthcare, Freiburg, Germany) according to the manufacturer's instructions. Briefly, cells were lysed in phosphate PBS containing 1 mM benzamidine and 4 mM PMSF. GST-C-Ift88 was eluted with 50 mM Tris–HCl pH 8.0, 10 mM Glutathione. GST-C-Ift88 was covalently coupled to CNBr activated Sepharose beads (GE Healthcare) according to the manufacturer's protocol. For pre-adsorption of unspecific antibodies, rabbit or guinea pig serum was successively incubated with CNBr activated Sepharose beads covalently coupled to BL21DE3 protein lysate or purified MBP. Specific anti-Ift88 IgGs were purified from pre-adsorbed sera using GST-C-Ift88 column.

2.4. SDS-PAGE and Immunoblotting

Lysates of brain tissue from *Ift88*$^{+/+}$ and *Ift88*$^{-/-}$ mice were separated on 10% SDS-PAGE and transferred onto nitrocellulose membranes (GE Healthcare). Immunoblots were probed with guinea pig and rabbit anti-Ift88 (1:250, 1:125, respectively) and mouse anti-actin (Millipore, 1:1000) as primary antibodies (Fig. 6T). Secondary antibodies were goat anti-mouse, goat anti-rabbit and goat anti-guinea pig IgGs conjugated to horseradish peroxidase (Dianova, Hamburg, Germany) 1:5000. Signals were detected by chemiluminescence on X-ray films.

2.5. Image acquisition

2.5.1. Widefield microscopy

Bright field images were acquired with a Leica DM1000 microscope using a 4× or a 10× objective. Images of immunofluorescent samples were acquired with an inverted fluorescence microscope (Axio Observer, Zeiss, Oberkochen, Germany) equipped for structured illumination (ApoTome, Zeiss) using 10×, 20×, 40× or 63× objectives (EC Plan-Neofluar, Zeiss) and the Zeiss Mosaix software if larger regions had to be imaged.

2.5.2. Confocal microscopy

Confocal microscopy was performed with a Nikon A1R microscope (Nikon Imaging Center, University of Heidelberg) using a 60× objective (NA 1.4) with oil immersion. Scans were taken at a 500 nm interval at a resolution of 1024×1024 pixels, using scan lines of 405, 491, and 561 nm.

2.5.3. 3D Structured Illumination Microscopy (3D-SIM)

Central midbrain stained for cilia structures (mouse anti-γ-tubulin and rabbit anti-Arl13b) were imaged on a 3D structured illumination microscope OMX v.4 (GE Healthcare). The reconstructed images show a resolution below the diffraction limit with an approximate lateral and axial resolution a factor two higher than conventional fluorescent microscopy at maximum magnification. Samples were mounted on high precision #1.5 coverglass (Marienfeld-Superior) in Vectashield (Vectors lab) and sealed with nail polish. The immersion oil was optimized according to its refractive index to avoid spherical aberrations in the green emission channel. The samples were sequentially structurally illuminated at 405 nm, 488 nm and 568 nm while sCMOS cameras recorded the corresponding emissions at the following bandwith of 436/31 nm, 528/48 nm and 609/37 nm. The Softworx v6.1.1. software (GE Healthcare) at a wiener filter setting of 0.004 with 528 nm emission channel optimized OTFs reconstructed the final images. Image intensities were adjusted linearly in order to minimize any visible spherical aberrations. Raw data is available upon request. 3D reconstruction were created with the Volocity software package (PerkinElmer).

2.6. Scanning Electron Microscopy (SEM)

Embryonic heads were fixed overnight at 4 °C in 2.5% glutaraldehyde/0.1M PIPES pH 7.4 and subsequently washed 3 times in 0.15 M PIPES, pH 7.4, at 4 °C. The fixed samples were then embedded in 3% agarose and cut into 300 μm coronal slices in PBS with a D.S.K. Microslicer. The slices were treated for 1 h at room temperature with 1% OsO4, washed 3 times with 0.15 M PIPES pH 7.4, and subsequently dehydrated in an ascending ethanol dilution series (50%, 70%, 90%, 100%). The specimens were dried in a CPD 030 critical point dryer (BAL-TEC AG, Liechtenstein) using CO_2 as a transitional medium, followed by sputter coating (BAL-TEC MED 020 sputter coater) of a 20 nm Gold film. For scanning electron microscopy (EM), a LEO 1530 field emission scanning electron microscope with a Schottky cathode was used (LEO Elektronmikroskopie, Oberkochen, Germany).

2.7. In situ hybridization

Radioactive *in situ* hybridization was performed as previously described (Brodski et al., 2003). Embryonic mice were immersion

fixed with 4% paraformaldehyde (PFA) and paraffin embedded. Antisense mRNA probes were transcribed from plasmids containing fragments of the murine tyrosine hydroxylase (*Th*) gene (base pairs 1–760; GenBank accession number M69200). Transcripts were radiolabeled by *in vitro* transcription with ^{35}S-UTP. For hybridization, sections were dewaxed, pretreated, and prehybridized. Subsequently, they were hybridized overnight at 57 °C and washed at 65 °C. The hybridized slides were dipped in autoradiographic emulsion (type NTB2; Eastman Kodak, Rochester, NY), developed after 6 weeks, and counterstained with cresyl violet.

Non-radioactive RNA *in situ* hybridization was essentially performed as previously described (Blaess et al., 2011). Frozen sections were fixed in 4% PFA and washed in PBS. Paraffin sections were deparaffinized, rehydrated, treated with Proteinase K (Roche, Penzberg, Germany) and then acetylated. After washing in H_2O, frozen and paraffin sections were dehydrated in different concentrations of ethanol (70%, 80%, 95% and 100%) and incubated in chloroform to de-fat the sections. After hybridization with the cRNA probes and immunodetection of digoxigenin with alkaline phosphatase conjugated antibody (Roche, Penzberg, Germany), sections were incubated with BM purple (Roche, Penzberg, Germany). The color reaction was stopped in Tris–EDTA buffer.

2.8. RNA isolation and quantitative real time RT-PCR

Total RNA was manually isolated from E11.5 microdissected midbrain tissue. RNA was extracted using RNeasy Mini Kit (74104 Qiagen, Hilden, Germany) according to the manufacturer's instructions. 1–5 μg of RNA was transcribed into cDNA using oligo(dT)$_{12-18}$ (0,5 μg/μl, Invitrogen, Life Technologies GmbH, Darmstadt, Germany) and random hexamers (50 mM, Applied Biosystems, Darmstadt, Germany) and SuperScript II RNase H$^-$ reverse transcriptase (Invitrogen). Quantitative real time PCR reactions were performed using the ABI Prism 7000 Detection System (Applied Biosystems) using TaqMan Gene Expression Assays (Applied Biosystems) with 1 μl cDNA. The following TaqMan Assays were used: *Wnt1* Mm01300555_g1, *Wnt5a* Mm00437347_m1, *Wnt7a* Mm00437354_m1, *Axin2* Mm01265783_m1, and *Ift88* (Mm01313467_m1). The standard quantification protocol was applied with the following cycles: 2 min at 50 °C, 10 min at 95 °C, followed by 45 cycles: 15 s at 95 °C and 1 min at 60 °C. Each individual reaction was performed in triplicate. GAPDH primers (Mm99999915_g1) were used to normalize results. Statistical analysis was performed as follows: Relative expression (RE) levels were calculated with the function ($RE = 2^{-\Delta\Delta Ct}$), where $\Delta\Delta Ct$ is the normalized difference in threshold cycle (Ct) number between wild-type and *Ift88* cko samples, calculated from the mean Ct value of triplicate replicates of any given condition. Statistical significance between wild-type and *Ift88* cko was evaluated by application of Student's *t*-test.

2.9. Quantification

The perimeter of Lmx1a- and FoxA2-positive domains were measured in E10.5 old embryonic midbrains ($n \geq 3$) using the ImageJ software package 1.48v (http://rsb.info.nih.gov/ij/ ⟨http://rsb.info.nih.gov/ij/⟩). The domains were normalized to the inner perimeter of the ventricle in each embryonic midbrain separately. To quantify the number of FoxA2- and TH-expressing mDA neurons at E13.5 and E18.5, at least three embryos per genotype were used. For E13.5, one intermediate section per embryo was counted that contained both, SN and VTA. For E18.5 embryos an anterior, intermediate and posterior section was counted for each embryo. For E18.5, numbers were normalized to wild-type (wild-type set at 100%). Note that 12 μm frozen sections were used for quantification of mDA neurons in E18.5 *Ift88* cko brains (controls: frozen sections), and 7 μm paraffin sections were used for quantification of mDA neurons in E18.5 *Gli2/3* cko brains (controls: paraffin sections). Counting was performed using the cell counter plugin in ImageJ.

2.10. Statistical analysis

Statistical analysis of histological data was performed using an unpaired two-sided Student's *t*-test and parametric analysis of variance (ANOVA) (Prism 6, Graphad). Statistical significance levels were set at $p < 0.05$ ($^*p < 0.05$, $^{**}p < 0.01$ $^{***}p < 0.001$). The values are represented as mean ± SD.

3. Results

3.1. Primary cilia are present on radial glia-like progenitors in the ventricular zone of the ventral midbrain

We and others have previously identified primary cilia in embryonic mouse midbrain, but the identity of the cells bearing the cilia was not determined (Lancaster et al., 2011; Willaredt et al., 2008). To address this question, we combined antibody staining for the proteins nestin and BLBP (brain lipid binding protein), which are both expressed by the radial glia-like mDA progenitors (Fig. 1E), and for the protein Arl13b (ADP-ribosylation factor like 13B), which is localized to the axoneme of primary cilia located at the ventricular zone (VZ) (Bonilla et al., 2008; Tang et al., 2009; Caspary et al., 2007; Kang et al., 2010). We could detect nestin-positive (Fig. 1A) or BLBP-positive (Fig. 1B) cells in the midbrain VZ that projected cilia into the ventricle of the embryonic day 12.5 (E12.5) ventral midbrain. To provide an independent investigation of the presence of primary cilia in the midbrain VZ, SEM was employed. Individual cilia with a length of about 1 μm could be detected projecting into the ventricles from cells at the ventricular surface in the ventral midbrain of E12.5 embryos (Fig. 1C and D).

3.2. The ventral midline and the mDA progenitor domain are disorganized in cbbs mutants

To test the functional importance of primary cilia in ventral midbrain and mDA development, we analyzed whether mDA progenitors and neurons develop in a mouse mutant with defective primary cilia. *Cobblestone* (*cbbs*) is a hypomorphic allele of the IFT gene *Ift88*, in which Ift88 mRNA and protein levels are reduced by 70–80% (Willaredt et al., 2008). Nevertheless it was reported previously that primary cilia are structurally normal in the forebrain VZ of *cbbs* mutants (Willaredt et al., 2008). To examine primary cilia in the *cbbs* mutants, antibody staining against Arl13b and γ-tubulin was employed, marking the axoneme and the basal body of cilia, respectively. Using super-resolution microscopy to visualize primary cilia, we found that structurally normal primary cilia were present at the VZ of the ventral midbrain in *cbbs* mutants (Fig. 2A and B, Movie 1 and 2).

Despite the presence of cilia, *cbbs* mutants are distinguished by multiple defects in development that phenocopy many of the abnormalities seen in the *Gli3^{Xtj}* mutant mice, including defects in Shh signaling in both embryonic forebrain (Willaredt et al., 2008) and heart (Willaredt et al., 2012). Thus, we first investigated whether Shh signaling is altered in the ventral midbrain of *cbbs* mutants. The induction of Shh-expression in the floor plate around E8.5 depends on high-level Shh signaling from the underlying notochord. In E11.5 wild-type embryos, *Shh* is expressed in a broad ventromedial domain, with strong expression laterally and weak expression medially (Fig. 3A). In the *cbbs* ventral midbrain, clusters of *Shh*-expressing cells were surrounded by *Shh*-negative cells (Fig. 3B and B′). To assess whether the surrounding cells were still

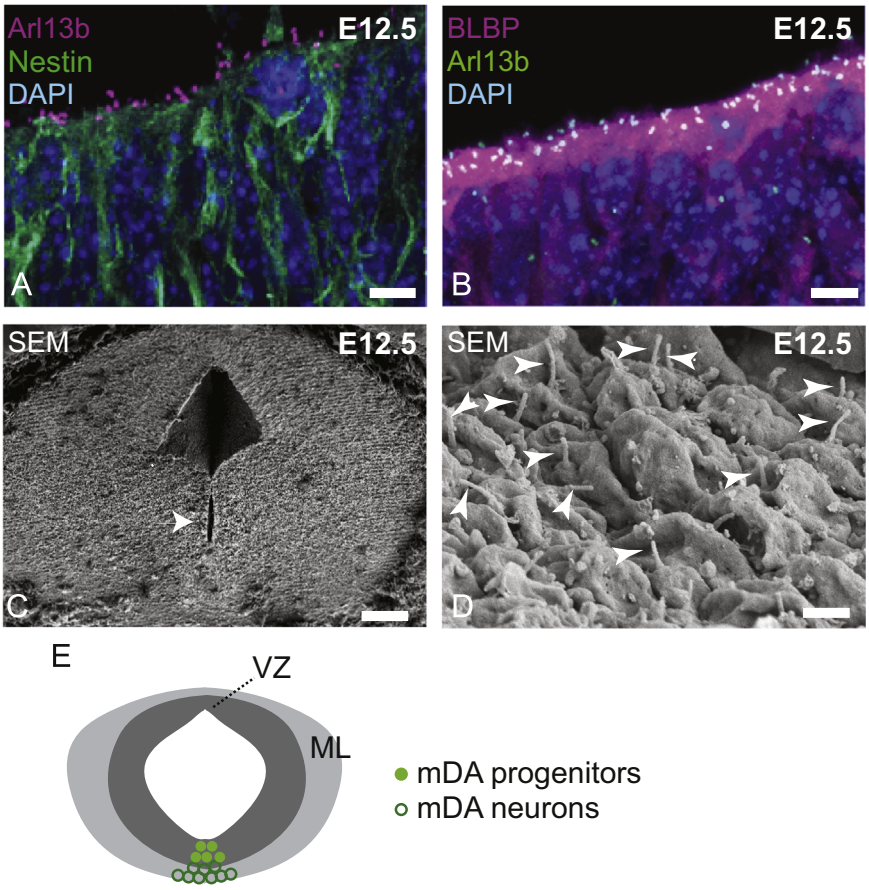

Fig. 1. Primary cilia are present on radial glia at the ventricular zone of the embryonic ventral midbrain. Immunofluorescent staining (A and B) and scanning electron microscopy (SEM) (C and D) of cilia projecting into the ventral mesencephalic ventricle of wild-type E12.5 embryos. A and B, Primary cilia were detected using an antibody against Arl13b (A, magenta, B, green). Neural progenitors were labeled with antibodies against nestin (A, green) or BLBP (B, magenta). Blue, DAPI-labeled nuclei. C and D: arrow in C indicates the ventral ventricular surface of the midbrain shown in D; arrowheads in D indicate primary cilia. Scale bars: A and B, 10 μm; C, 500 μm; D, 1 μm. (E) Schematic representation of the location of mDA progenitors and neurons in the E12.5 midbrain.

responsive to Shh signaling, we analyzed the expression of the zinc-finger transcription factor *Gli1*, an activator in the Shh signaling pathway, whose expression is positively regulated by Shh signaling, thus serving as a readout for active Shh signaling. In the wild-type midbrain, two ventrolateral *Gli1* positive domains are located juxtaposed to the *Shh*-positive domain (Fig. 3A and C). *Gli1* expression is excluded from the *Shh*-expressing domain itself, since the components of the canonical Shh signaling pathway are downregulated in this area (Fig. 3A, C and G) (Mavromatakis et al., 2011). In *cbbs* mutants, *Gli1* was expressed throughout the ventral midline region, but was excluded from the *Shh*-positive cell clusters (Fig. 3D and D′), indicating that the Shh signaling pathway was activated in ventral midline cells in the mutants. Next we investigated *Gli3* expression, which is negatively regulated by high-levels of Shh signaling. Consequently, *Gli3* is restricted to the dorsal midbrain in control embryos (Fig. 3E and E′). The *Gli3* positive domain was expanded ventrally in *cbbs* mutant embryos, and clusters of *Gli3*-positive cells were located in the ventral midline region and within the *Gli1* positive area (Fig. 3F and F′).

In addition to the abnormal intermixing of *Shh*-, *Gli1*-, and *Gli3*-expresssing progenitors in the ventral midbrain of *cbbs* mutants, cell organization and morphology was altered. *Shh*-positive/*Gli1*-negative cells were sometimes organized in rosette-like structures and the tissue architecture appeared to be disorganized (Fig. 3B,B′, D,D′,F,F′,I and I′), as previously noted in the forebrain of this mutant (Willaredt et al., 2008). The cyclin D1-positive VZ was thicker in the *cbbs* mutant (Fig. 3K and K′) than in the wild-type littermates (Fig. 3J and J′) and was not clearly separated from the emerging mantle layer (Fig. 3H–I′).

3.3. *mDA progenitors and neurons are massively reduced in cbbs mutants*

The induction of mDA progenitors in the ventral midline of the midbrain depends on Shh signaling (Blaess et al., 2006). In *cbbs* mutants, Shh signaling was still activated. However, the organization of Shh-expressing and responding domains was severely disrupted. We next assessed whether the disorganization of the ventral midline VZ might have a negative impact on the generation of mDA progenitors. In the wild-type embryo the transcription factors Lmx1a and Foxa2 are expressed in the mDA progenitor domain, while the transcription factor Nkx6-1 is not expressed (Fig. 4A, C and M) (Andersson et al., 2006). An adjacent, lateral progenitor domain, which gives rise to cells of the midbrain red nucleus, is Foxa2- and Nkx6-1-positive, but Lmx1a negative (Fig. 4A, C and M) (Prakash et al., 2009). More laterally, progenitors

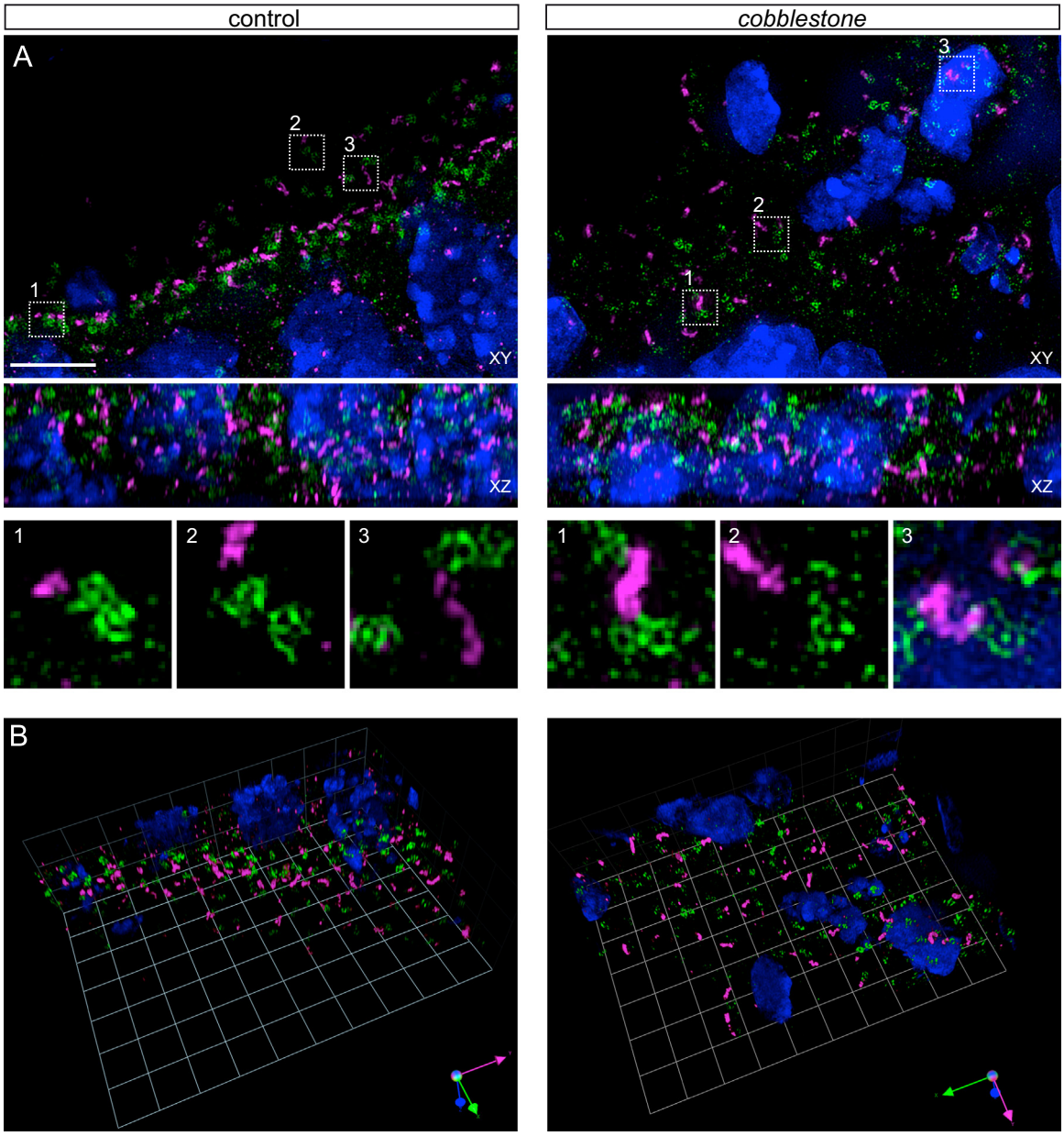

Fig. 2. Super-resolution microscopy of primary cilia in the ventral midbrain of E11.5 wild-type and *cobblestone* embryos does not show major structural differences in the primary cilia or basal bodies. (A) Primary cilia were detected using an antibody against Arl13b (magenta). Basal bodies were detected using an antibody against γ-tubulin (green). Blue, Hoechst-labeled nuclei. Note that the number of visible nuclei does not reflect the total number of cells that make contact with the ventricular surface and extend primary cilia into the ventricle. The top image depicts a 30 μm (*x*) by 20 μm (*y*) maximum-intensity *z*-projection of a 7.25 μm-thick image stack. Bottom image is a maximum intensity *y*-projection of the corresponding *xz* slices of the recorded volumes. Higher magnifications of the boxed areas are shown in the bottom. Scale bar: 5 μm. (B) 3-dimensional reconstruction of the corresponding $30 \times 20 \times 7.25\ \mu m^3$ (*xyz*) image stacks. The squares are 3 μm in length.

are Nkx6-1 positive, but Foxa2 and Lmx1a negative (Fig. 4A, C and M). In E11.5 *cbbs* mutants, cells with the expression profiles of these progenitor domains were intermingled in the ventral midline (Fig. 4B and D). The Lmx1a-positive cells were located off-midline, in areas that contained predominantly Foxa2-positive, Nkx6-1-negative cells (Fig. 4B′′). These Lmx1a-positive cells were found at a distance to the ventricle, consistent with the disorganized VZ in the ventral midbrain of *cbbs* mutants (compare Fig. 3K and K′). Moreover, we could not detect Lmx1a expression in the ventral midbrain of E10.5 *cbbs* mutant embryos (Fig. 4I and J), suggesting a delay in the induction of mDA progenitors. The induction of Lmx1a expression in mDA progenitors is dependent on Wnt1 signaling (Yang et al., 2013), and there is plenty of evidence that Wnt signaling can depend on the function of primary cilia (Oh and Katsanis, 2012). We therefore examined whether *Wnt1* expression and signaling is altered in *cbbs* mutants. Neither *Wnt1* nor *Axin2*, a readout for canonical Wnt signaling (Jho et al., 2002), were expressed in the ventral midbrain of *cbbs* mutants (Fig. 4E–H). Finally, we investigated whether the floor plate markers Corin and Arx were expressed in the *cbbs* mutants. Between E10.5 and E12.5, we could detect Arx and Corin in the ventral midbrain of some but not all mutants ($n=3/5$ for Corin; $n=2/4$ for Arx). *Arx* and *Corin* expression were located within the Foxa2 positive domain and, at E12.5, overlapped with Lmx1a expression (Fig. 4I–L, Supplemental Fig. 1). In summary, these results show that the integrity of the progenitor domains of the ventral

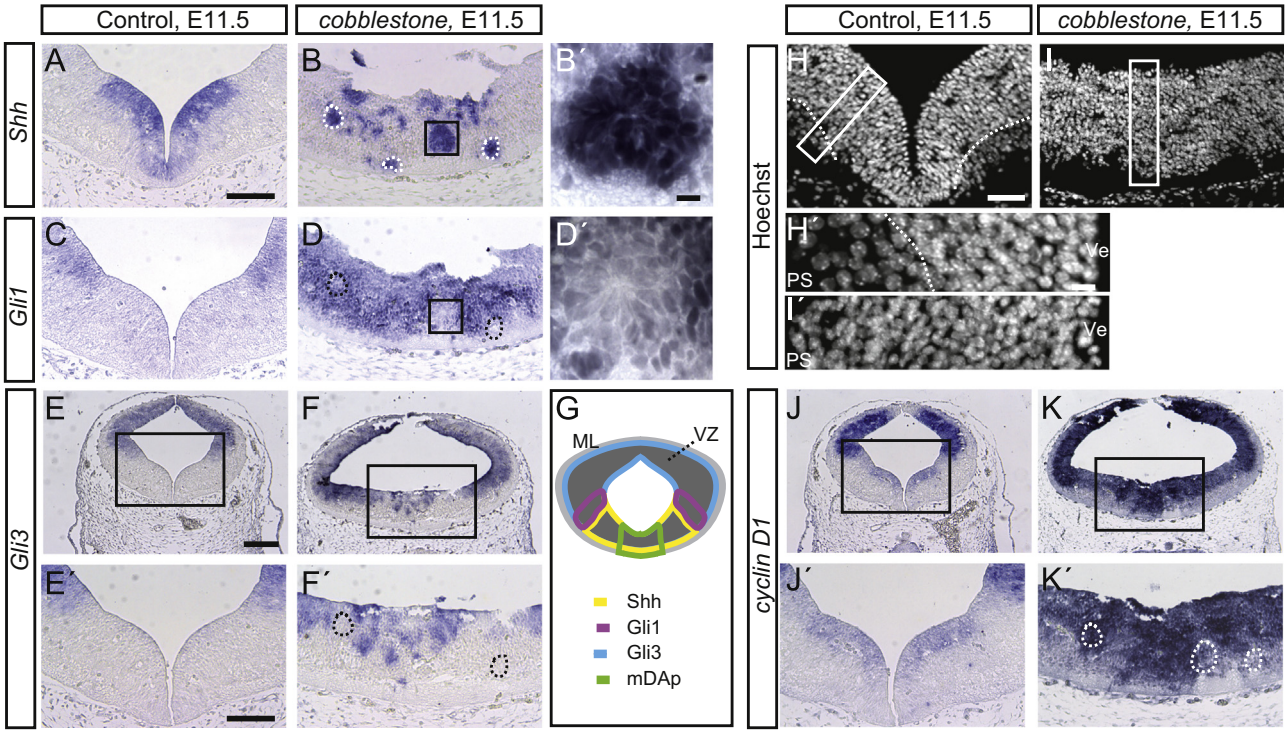

Fig. 3. Disorganization of the mDA progenitor domain in *cobblestone* mutant mice. (A–F′, J–K′) RNA in situ hybridization for *Shh* (A–B′), *Gli1* (C–D′), *Gli3* (E–F′), and *Cyclin* D1 (J–K′) showing clusters of progenitor cells. (G) Schematic overview of the relevant gene expression domains in the wild-type ventral midbrain. (H–I′) Hoechst-labeled nuclei within the ventral midbrain show disorganization of the mDA progenitor domain in *cobblestone* mutant mice. (B′,D′–F′,H′–K′) are higher magnifications of the boxed areas in (B,D–F,H–K). Ve: Ventricle; PS: Pial surface. Scale bars: A–D,E′,F′,H,I,J′,K′, 100 μm; B′,D′,H′,I′, 20 μm; E,F,J,K, 200 μm.

midbrain, Wnt signaling, and the induction of mDA progenitors is severely impaired in the *cbbs* mutant, whereas residual Shh signaling is maintained.

Next we investigated whether differentiated mDA neurons are generated from the presumptive Lmx1a/Foxa double-positive mDA progenitor domain in *cbbs* mutants. In addition to Lmx1a, differentiated mDA neurons express Foxa2, the transcription factors Nurr1 (Nuclear receptor related 1) and Pitx3 (Paired-like homeodomain transcription factor 3) and the rate-limiting enzyme in dopamine synthesis, tyrosine hydroxylase (TH) (Blaess and Ang, 2015) (Fig. 5G, I, K and P). In E12.5 *cbbs* mutants we could detect few neurons positive for TH (Fig. 5B, D and F), compared to control littermates (Fig. 5A, C and E). These TH-expressing neurons were Lmx1a- and Foxa2-positive and co-expressed Nurr1 and Pitx3, indicating that they were properly specified towards a mDA neuronal fate (Fig. 5H, J, L–N). These TH-positive neurons were sometimes clustered at the periphery of rosette-like structures (Fig. 5M-O). Immunofluorescent staining for the primary cilia marker Arl13b and axoneme protein γ-tubulin showed that primary cilia extended into the center of these rosettes (Fig. 5 M). We could not examine whether TH-positive neurons developed into fully mature mDA neurons, since *cbbs* mutants seldom survive past E14.5 (Willaredt et al., 2012, 2008).

3.4. *Conditional inactivation of Ift88 results in loss of primary cilia, complete inactivation of Shh signaling, and impaired Wnt signaling in the ventral midbrain*

Since the *cbbs* allele is hypomorphic, expressing an Ift88 protein with a normal amino-acid sequence at only 25% the level of wildtype littermates, we next investigated how the complete loss of functional cilia in the midbrain affects the induction and specification of mDA progenitors and the generation of mDA neurons. To this end, we conditionally inactivated *Ift88* in the midbrain and anterior hindbrain after E8.5 by crossing the $En1^{Cre}$ line (Kimmel et al., 2000) to a floxed allele of *Ift88* (Haycraft et al., 2007) (*Ift88* cko) (Fig. 6A). To examine whether and when primary cilia were lost in the midbrain of *Ift88* cko embryos, *Ift88* cko and control embryos were examined at progressive developmental stages starting from E9.5 (Fig. 6B–I). Primary cilia were co-labeled with an anti-γ-tubulin antibody to recognize the basal body and an anti-Arl13b antibody to label the ciliary axoneme. At E9.5, we observed a significant loss of primary cilia from the ventricular surface (Fig. 6D and E), which was complete at E10.5 (Fig. 6F and G). This was paralleled by a drastic loss of Ift88-positive cilia at the ventricle of E10.5 embryos, as seen with a co-labeling of anti-Ift88 and anti-γ-tubulin antibodies (Fig. 6B and C). In addition, examination of E12.5 *Ift88* cko mutants with SEM revealed a complete loss of primary cilia projecting into the ventricle (Fig. 6H and I, compare with Fig. 1C and D). Effectiveness of gene inactivation was further indicated by examination of *Ift88* mRNA levels in microdissected E11.5 midbrain tissue, which showed a reduction of 88.8% ± 2.7% ($p < 0.0001$) in mutants compared to controls. To assay the specificity of the inactivation, primary cilia were also examined in the forebrain of E12.5 *Ift88* cko mutants. Normal numbers of primary cilia were found both in the cerebral cortex and in the diencephalon, as detected by immunostaining for Arl13b and by SEM (data not shown).

We next assessed whether and when Shh signaling was inactivated in *Ift88* cko mutants (Fig. 6J–S). In E9.5 and E10.5 *Ift88* cko mutants, *Gli1* expression was absent (Fig. 6K and N), while the *Gli3* domain was expanded towards the ventral midline (Fig. 6Q and S). These results indicate that Shh signaling was indeed abolished in the *Ift88* cko mutants already at E9.5, corresponding with a major loss of primary cilia at the VZ at this stage (Fig. 6C).

To investigate whether Wnt signaling was also affected in the *Ift88* cko mutants, we examined mRNA levels of *Wnt1, Wnt5a* and *Wnt7a* in microdissected E11.5 midbrain tissue comparing *Ift88* cko and littermate controls using real-time quantitative qPCR. We found that mRNA levels of all three Wnt family members

were reduced in the *Ift88* cko mutants (*Wnt1*: 41.45% ± 4.8% (p=0.0033), *Wnt5a*: 60.2% ± 6.4% (p=0.0026) *Wnt7a*: 11.78% ± 1.6% (p=0.0054)). A reduction of *Wnt1* expression in *Ift88* cko embryos was also seen by examination through in situ hybridization (Fig. 7J and K). Expression of *Axin2*, which serves as a readout for canonical Wnt signaling, was also reduced by 62.4% ± 7.5% (p=0.0037; for all comparisons: Student's t-test; n=4) compared to wild-type controls.

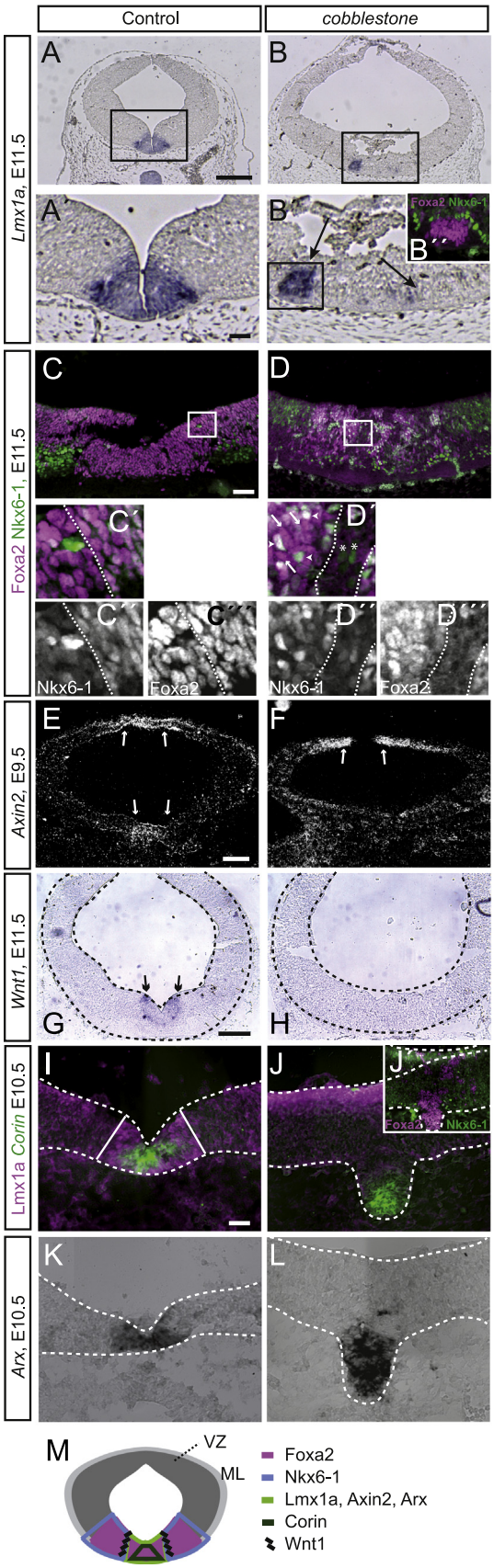

3.5. *Ift88 is required for establishing ventral progenitor domains in the developing midbrain*

We next investigated whether the conditional inactivation of *Ift88* after E9.0 and the resulting loss of primary cilia leads to defects in the mDA progenitor domain (Fig. 7R). At E10.5, Shh and Foxa2 expression overlapped in a broad ventral domain in the wild-type (Fig. 7A, D and M). The size of the Shh- and Foxa2-positive domains were significantly reduced in the *Ift88* cko embryos (Fig. 7B, E, N and P). The expression domain of Lmx1a (Fig. 7G) was also decreased in size in the *Ift88* cko embryos compared to control (Fig. 7H and Q). In contrast, Nkx6-1, which is expressed lateral to the Lmx1a domain (Fig. 7R), was not obviously altered (Fig. 7M and N). However, because of the small Foxa2 domain, the Foxa2/Nkx6-1-double positive domain was almost completely lost in the *Ift88* cko embryos (Fig. 7M and N). Together, these data indicate that Ift88 is necessary after E9.0 to establish a broad Shh/Foxa2-positive expression domain in the ventral midbrain. *Ift88* is not required after E9.0 to induce the mDA progenitor domain, but it is involved in regulating the size of this domain.

3.6. *mDA neurons are reduced in absence of Ift88*

Since we observed that the size of the Lmx1a-positive mDA progenitor domain was decreased in *Ift88* cko mice, we investigated whether the number of mDA neurons was reduced in these mutant mice. At E13.5, most mDA neurons are already differentiated and express TH (Bayer et al., 1995). The comparison of *Ift88* cko and control brains demonstrated a significant loss of TH-positive neurons in the ventral midbrain of *Ift88* cko embryos (Fig. 8B) compared to the control (Fig. 8A; WT: 928.8 ± 64.1 cells, *Ift88* cko: 627.5 ± 21.7 cells, n=4, Student's t-test: p=0.0043). In particular, medially-located mDA neurons appeared to be missing in the mutant embryos (Fig. 8A and B). Nevertheless, the observed TH-positive neurons co-expressed FoxA2, suggesting that they displayed the proper mDA neuronal phenotype (Fig. 8C–F, E′ and F′). To investigate whether this phenotype persists at later stages, we performed an immunostaining for TH and FoxA2 on E18.5 midbrains. At this stage, the medially located VTA and the laterally located SN could be distinguished. Compared to the E18.5 control brains (Fig. 8G), the VTA and SN were less densely populated by TH- and Foxa2-positive mDA neurons and the overall number of TH-positive neurons was significantly reduced in the *Ift88* cko midbrain (Fig. 8H and R). To confirm that the TH-positive neurons had adopted a proper mDA identity at E18.5, we

Fig. 4. Expression profiles of progenitor domains are intermingled in *cobblestone* mutants. (A and B) RNA *in situ* hybridization for *Lmx1a* on coronal midbrain sections of wild-type and *cobblestone* mutant embryos at E11.5. (A′ and B′) higher magnification of boxed areas in A,B, respectively. Inset in B': Immunofluorescence for FoxA2 (magenta) and Nkx6-1 (green) on adjacent sections (B′′). (C–D′′′), Immunofluorescence for neural progenitor markers FoxA2 (magenta) and Nkx6-1 (green). C′–D′′′, higher magnification of boxed areas in C, D. (E–H) RNA *in situ* hybridization for *Axin2* (E,F) and *Wnt1* (G,H) on coronal midbrain sections of wild-type and *cobblestone* mutant embryos at E9.5 (E,F) and E11.5 (G,H). (I and J) RNA *in situ* hybridization for *Corin* (green) combined with immunofluoresence for Lmx1a (magenta) (I,J) and RNA *in situ* hybridization for *Arx* (K,L) on coronal midbrain sections of wild-type and *cobblestone* mutant embryos at E10.5. Note that the image of the *Corin* RNA *in situ* hybridization was false colored and image color was inverted to visualize overlap with Lmx1a. *Corin* and *Arx* expression could be detected in the ventral midbrain in one of three E10.5 embryos, while Lmx1a expression was absent in all analyzed embryos. (M) Schematic overview of expression domains of FoxA2, Nkx6-1 and Lmx1a in the wild-type ventral midbrain. Scale bars: A, B, 200 μm; A′, B′, C, I–L, 40 μm, E–H, 100 μm.

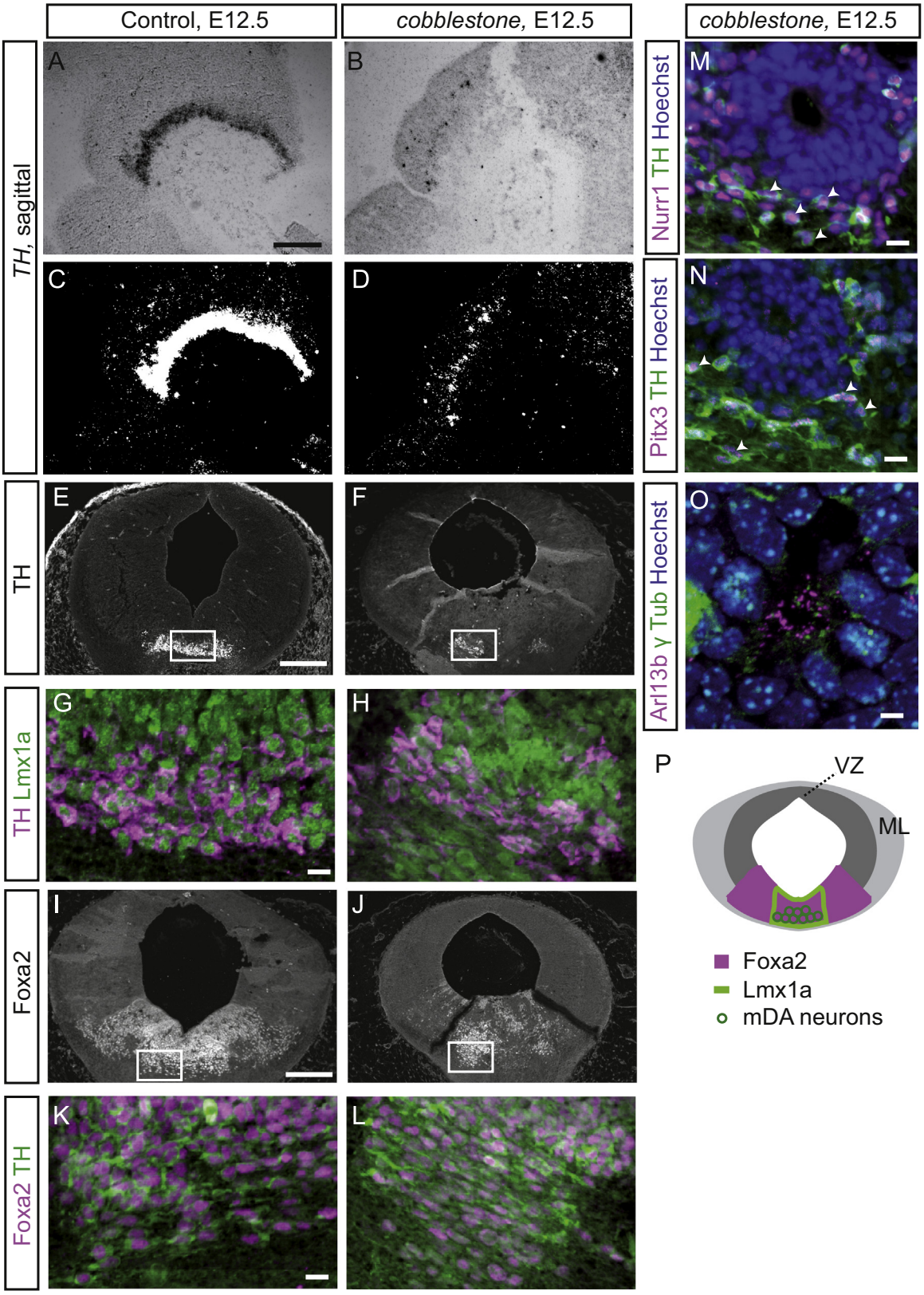

Fig. 5. Number of mDA neurons is severely reduced in *cobblestone* mutants. (A–D) RNA in situ hybridization for *TH* to visualize mDA neurons on sagittal sections of control and *cobblestone* mutant embryos at E12.5. (E–L) Immunofluorescent staining for TH on coronal midbrain sections in wild-type and *cobblestone* mutant embryos at E12.5. Co-staining with Lmx1a (G, H) and FoxA2 (I–L). (M, N) Immunofluorescent staining for TH and Nurr1 (M) or TH and Pitx3 (N) shows that mDA neurons surround rosette-like structures in the *cobblestone* mutant. (O) Immunofluorescent staining for primary cilia marker Arl13b and axoneme protein γ-tubulin shows that the primary cilia extend into the center of the rosette like structures. Blue, Hoechst-labeled nuclei. P, Schematic representation of FoxA2 and Lmx1a expression domains and localization of mDA neurons in the wild-type. Scale bars: A–F, I, J, 200 μm; G,H, K–N, 20 μm; O, 10 μm.

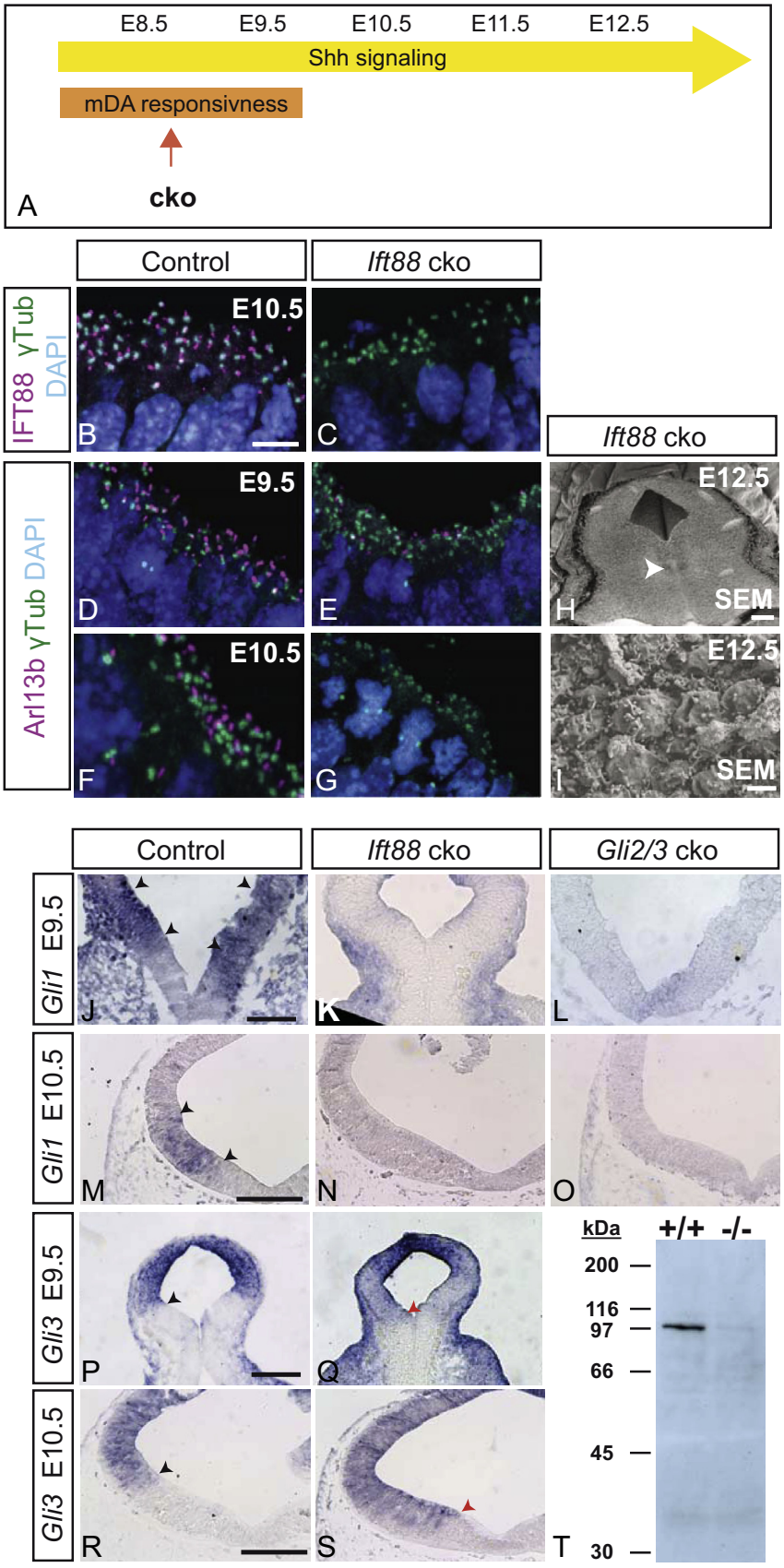

Fig. 6. Conditional inactivation of *Ift88* leads to a loss of primary cilia and impaired Shh signaling. (A) Schematic representation of the timeline of Shh signaling, mDA progenitor responsiveness to Shh signaling and timepoint of conditional gene inactivation (cko). (B–G) Immunofluorescent staining for Ift88 (B, C, magenta) or ciliary marker Arl13b (D–G, magenta) and γ-tubulin (B–G, green) at the ventricular surface of the ventral midbrain of control and *Ift88* cko embryos at E9.5 or E10.5. Blue, Hoechst-labeled nuclei. (H,I) SEM of the ventral midbrain at E12.5 in *Ift88* cko embryos. Arrowhead in H indicates the area imaged in I. In *Ift88* cko embryos, primary cilia start to disappear at E9.5 and are lost completely at E10.5. (J–S) RNA in situ hybridization for *Gli1* (J–O) and *Gli3* (P–S) on control, *Ift88* cko and *Gli2/3* cko embryos at E9.5 (J–L,P,Q) and E10.5 (M–O, R,S). Black arrowheads indicate the domain in the control, red arrowheads indicate the changes in the expression domain in the *Ift88* cko embryos. Similarly to *Gli2/3* cko, *Ift88* cko mutant embryos show a loss in Shh-responsiveness (*Gli1* expression). (T) Western blot of protein lysates of E12.5 brain from wild-type (+/+) and *cbbs*/*cbbs* (-/-) embryos, using an anti-C-terminal Ift88 antibody.Scale bars: B–G, 10 μm; H, 500 μm; I, 1 μm; J–S, 200 μm.

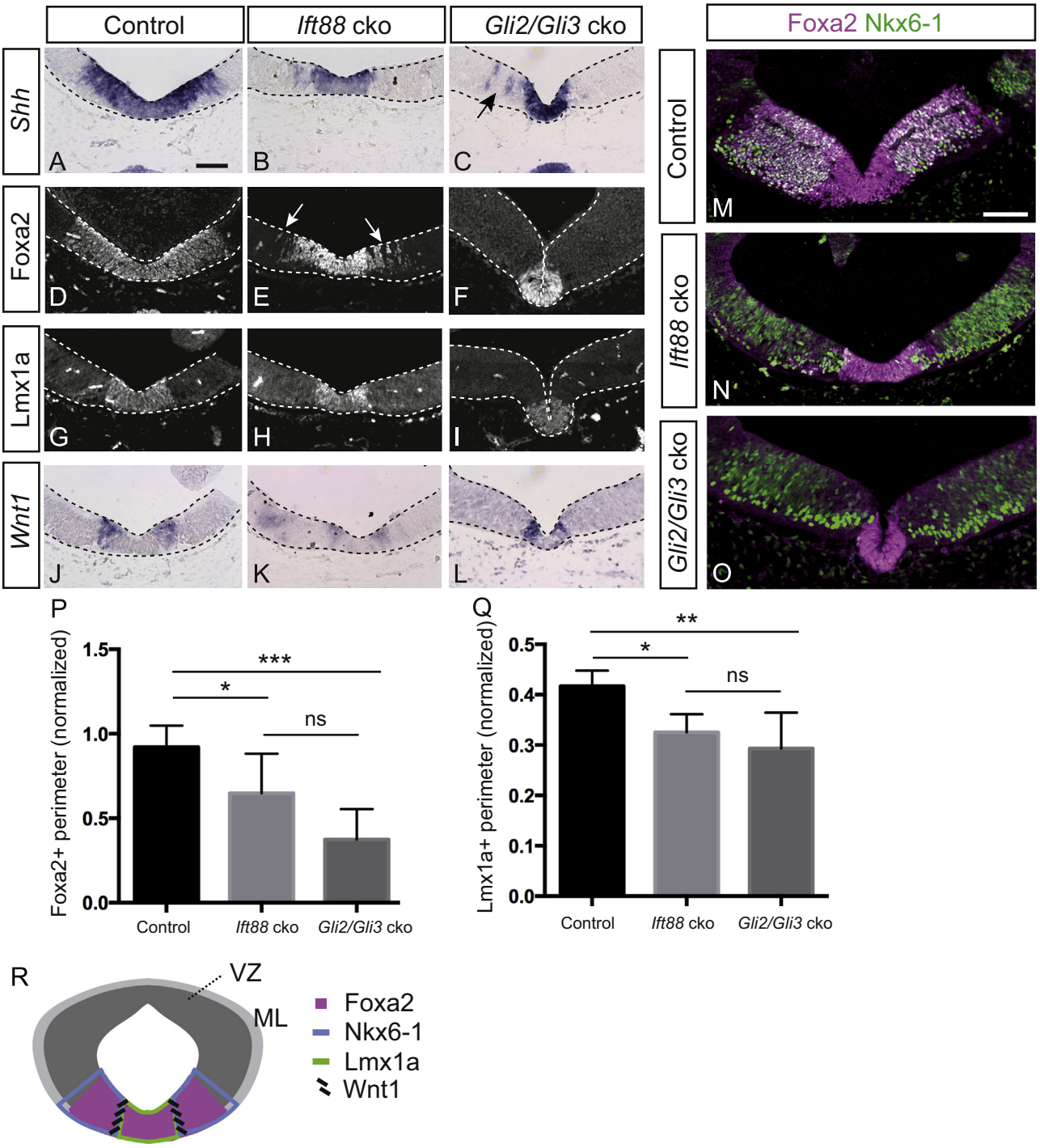

Fig. 7. The size of the mDA progenitor domain is reduced in *Ift88* cko and *Gli2/3* cko mutant embryos. (A–L) *RNA* in situ hybridization for *Shh* (A–C), *Wnt1* (J–L) and immunofluorescence staining for FoxA2 (D–F) and Lmx1a (G–I) on ventral midbrain sections of wild-type, *Ift88* cko and *Gli2/3* cko embryos at E10.5. The VZ is outlined. Arrowheads in C,E point to striped expression patterns of *Shh* and FoxA2 in the mutants. (M–O) Immunofluorescent staining for FoxA2 and Nkx6-1. The progenitor cells co-expressing FoxA2 and Nkx6-1 are absent in *Ift88* cko and *Gli2/3 cko* embryos. (P,Q) Quantification of the size of the FoxA2- (P) and Lmx1a-positive (Q) domains in E10.5 control, *Ift88* cko and *Gli2/3* cko embryos. Values are means ± SD. The perimeter of the Lmx1a or Foxa2 positive domain was measured and normalized for the perimeter of the ventricle. ANOVA with Tukey's multiple comparison test. $n \geq 3$. Foxa2: $F_{(2,13)}=12.63$, Lmx1a: $F_{(2,8)}=8.67$, * $p<0.05$, ** $p<0.01$, *** $p<0.001$. (*R*) Schematic representation of expression domains of the markers given in A–O. Scale bars: 100 μm.

analyzed whether they co-expressed the transcription factors Nurr1 and Pitx3 as well as dopamine transporter (DAT), vesicular monoamine transporter 2 (Vmat2), and aromatic L-amino acid decarboxylase (Aadc) (Blaess and Ang, 2015). Indeed, we found that TH-positive neurons co-expressed all these markers (Fig. 8J–Q).

3.7. Conditional inactivation of Ift88 results in a phenotype comparable to conditional inactivation of the Gli2 and Gli3 transcription factors

The *Ift88* cko mutants show a complete loss of Shh signaling in the ventral midbrain after E9.0, but also a reduction in Wnt signaling. Since both pathways are important for generation of mDA neurons, we next assessed whether loss of Shh signaling is the primary cause for the defects in the generation of mDA progenitors and neurons seen in *Ift88* cko mice. Thus, we abolished the Shh

signaling by inactivating *Gli2* and *Gli3* using $En1^{Cre}$ ($En1^{Cre/+}$, $Gli2^{zfd/flox}$, $Gli3^{xt/flox}$, referred to as *Gli2/3* cko) and compared the resulting phenotype with the phenotype of the *Ift88* cko mice. We inactivated both *Gli2* and *Gli3* since loss of cilia interferes with the Shh signaling pathway on the level of these Gli proteins. In the absence of cilia neither Gli2/3 activators nor Gli3 repressors are formed (Haycraft et al., 2005; Huangfu and Anderson, 2005; Liu et al., 2005; Santos and Reiter, 2014). Moreover, only in the absence of both Gli2 and Gli3 (Bai et al., 2004) is Shh signaling completely abolished. Reflecting this, *Gli1* expression could not be detected in the midbrain of *Gli2/3* cko embryos at E9.5 or E10.5 (Fig. 6L and O).

Analysis of the ventral midbrain progenitor domains in *Gli2/3* cko embryos showed that the size of the *Shh*/Foxa2- double-positive domain was severely reduced in *Gli2/3* cko (Fig. 7C, F, N and P) compared to the control (Fig. 7A, D, M and P). In addition, the expression domain of the mDA progenitor marker Lmx1a (Fig. 7I and Q) was reduced in size in *Gli2/3* cko embryos compared to controls (Fig. 7G). The domain co-expressing FoxA2 and Nkx6-1, which is present in the wild-type (Fig. 7M), was completely lost in *Gli2/3* cko midbrains because of the severely reduced size of the FoxA2-positive area (Fig. 7O) and the *Wnt1* expression domain was shifted towards the ventral midline in *Gli2/3* cko midbrains, but expression levels were not obviously decreased (Fig. 7L). As expected from the severe reduction of the progenitor domain, TH-positive mDA neurons were reduced in *Gli2/3* cko mutant mice at E12.5 (WT: 456.7 ± 45.4 cells, *Ift88* cko: 254.7 ± 57.2 cells, $n=3$, Student's *t*-test: $p=0.05$) and at E18.5 (Fig. 8I, I′ and S). The reduction was essentially identical to the one observed in *Ift88* cko mutants (Fig. 8H, H′ and R).

3.8. Downstream signaling from a constitutively-active Smoothened mutant in embryonic midbrain is completely dependent upon functional primary cilia

The midbrain phenotype of the *Ift88* cko mice largely resembles the phenotype in *Gli2/Gli3* cko embryos. These data suggests that cilia-dependent loss of Shh signaling is the main cause of the

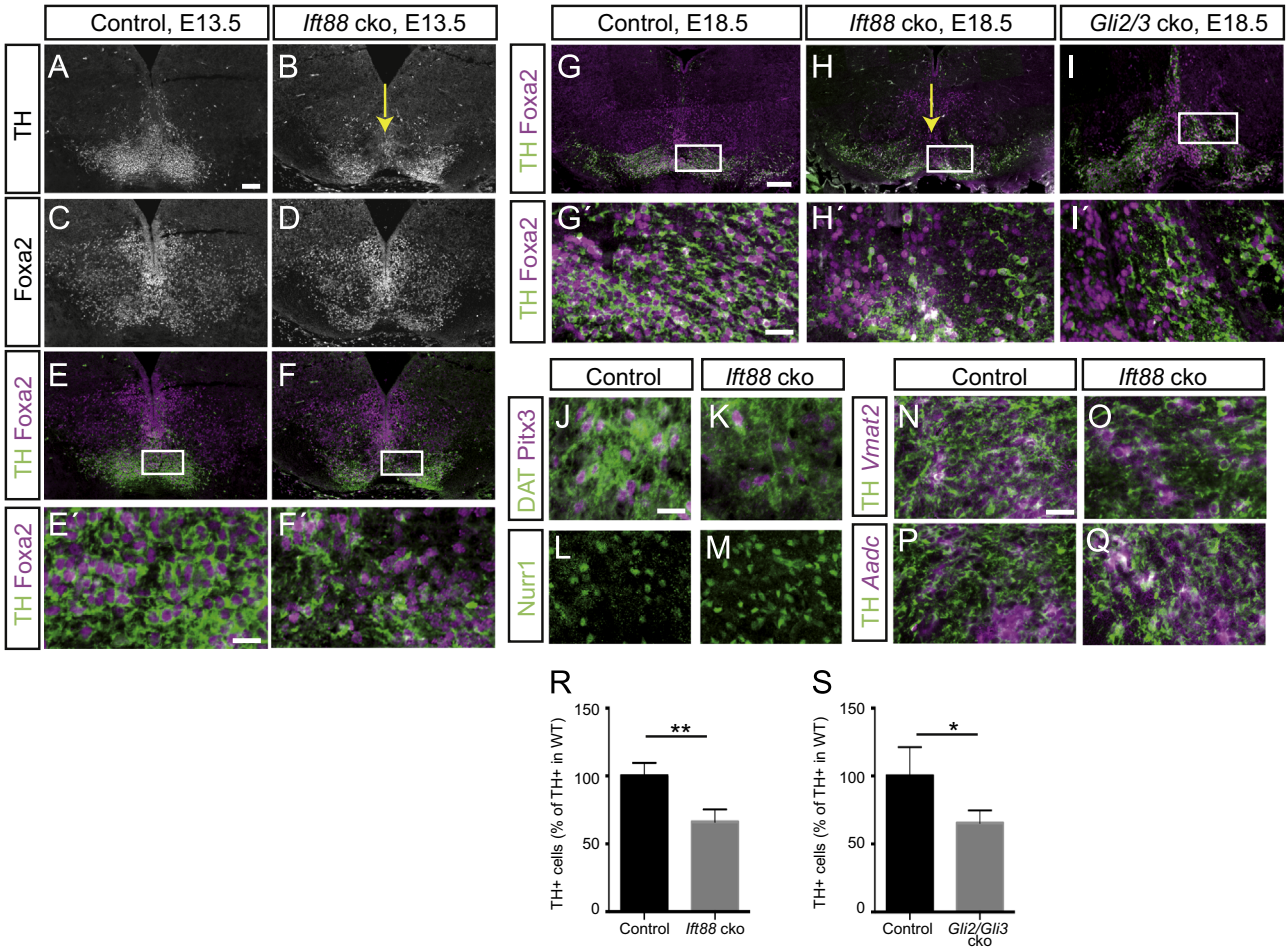

Fig. 8. mDA neurons are reduced in *Ift88* cko and *Gli2/3* cko mutant embryos. (A–F′) Immunofluorescent staining for TH and FoxA2 on control and *Ift88* cko ventral midbrains at E13.5. (E′,F′), higher magnification of boxed areas in E,F. Yellow arrow indicates the loss of mDA neurons in the midline. (G–I′) Immunofluorescent staining for TH and FoxA2 on wild-type, *Ift88* cko and *Gli2/3* cko ventral midbrains at E18.5. (G'-I') Higher magnification of boxed areas in G–I. Yellow arrow indicates the loss of mDA neurons in the midline. (J–M) Immunofluorescent staining for DAT and Pitx3 (J, K) and for Nurr1 (L, M) on E18.5 control and *Ift88* cko ventral midbrain coronal sections. (N–Q) Immunofluorescent staining for TH and RNA *in situ* hybridization for *Vmat2* and *Aadc*. Note that the image of the *Vmat2* and *Aadc* RNA *in situ* hybridization signal was false colored and image color was inverted to visualize overlap with TH. (R, S) Quantification of TH-positive cells in control versus *Ift88* cko (R) and control versus *Gli2/3* cko brains at E18.5 (S). The number of TH-positive cells is significantly reduced in *Ift88* cko and *Gli2/3* cko embryos as compared to wild-type. Values are given as mean percentage from wild-type TH-positive cells ± SD. Student's *t*-test: *Gli2/3* cko: $n \geq 3$, $t(6)=2.60$, *Ift88* cko: $n \geq 3$, $t(7)=4.99$, $^*p < 0.05$, $^{**}p < 0.01$. TH-positive neurons were quantified in 14 μm frozen sections for *Ift88* cko embryos and control littermates and in 7 μm paraffin sections for *Gli2/3* cko embryos and control littermates. Thus, the results are represented independently. Scale bars: A–F, 100 μm; G–I, 200 μm; G′–J′, N–Q 40 μm; E′,F′, J–M, 20 μm.

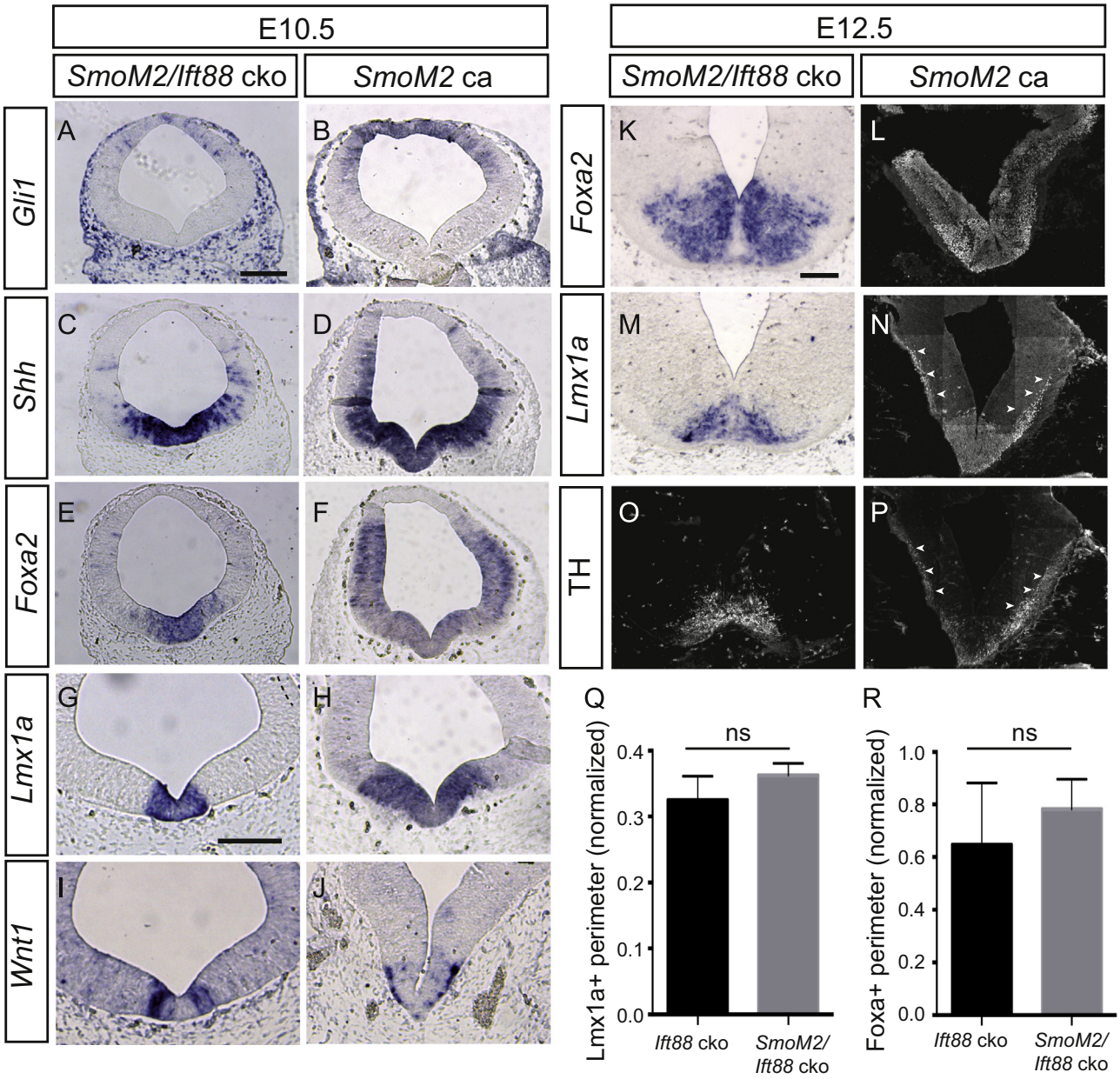

Fig. 9. Primary cilia are required for Shh pathway activation downstream of Smo. (A–K, M) RNA *in situ* hybridization for *Gli1* (A,B), *Shh* (C, D), *FoxA2* (E, F, K), *Lmx1a* (G, H, M) and *Wnt1* (I, J) on *SmoM2/Ift88* cko and *SmoM2* ca mutant embryos at E10.5 (A–J) and E12.5 (K–P). (L, N–P) Immunofluorescent staining for FoxA2 (L), Lmx1a (N), and TH (O,P) on *SmoM2/Ift88* cko and *SmoM2 ca* embryos at E12.5. (Q, R) Quantification of the size of the Lmx1a- (Q) and Foxa2-positive (R) domains in E10.5 *Ift88* cko and *SmoM2/Ift88* cko embryos. Values are means ± SD. The perimeter of the Lmx1a or Foxa2 positive domain was measured and normalized for the perimeter of the ventricle. Values are means ± SD. Student's *t*-test. Foxa2 domain: $n \geq 3$, $t(5)=0.90$, Lmx1a domain: $n \geq 3$, $t(4)=1.60$. Constitutive activation of the Shh pathway results in the ventralization of the midbrain and an abnormal distribution of mDA progenitors and neurons. Conditional inactivation of *Ift88* on the *SmoM2* background (*SmoM2/Ift88* cko) results in a phenotype similar to *Ift88* cko embryos indicating that primary cilia are necessary for Shh pathway activation downstream of Smo. Compare with Figs. 7 and 8 for controls and *Ift88* cko brains. Scale bars: A–J, 200 μm; K–P, 100 μm.

reduced size of the mDA progenitor domain in *Ift88* cko mutants. To investigate whether the main effect of the cilia loss impacts on the formation of Gli activator and repressor, we expressed a constitutively-active *Smo* mutant construct in the midbrain of *Ift88* cko mice after E8.0 ($En1^{Cre/+}$; $R26^{SmoM/+}$; $Ift88^{flox/flox}$ termed *SmoM2/Ift88* cko). These mice were compared with mice in which a constitutively-active *Smo* was expressed in a wild-type background ($En1^{Cre/+}$; $R26^{SmoM/+}$ termed *SmoM2* ca). Constitutive activation of the Shh pathway in the entire midbrain in *SmoM2* ca mice resulted in the ventralization of the midbrain. This was evident by the dorsal expansion of the *Foxa2*- and *Shh*- double positive domain and the dorsal shift of the *Gli1*-positive domain in the midbrain of E10.5 *SmoM2* ca embryos (Fig. 9B, D and F compare to control in Figs. 6M and 7A, D and P). However, the *Lmx1a* and *Wnt1*-positive domain was still restricted to the ventral midbrain, but was increased in size, and *Wnt1* was abnormally distributed compared to controls (Fig. 9H and J, compare to control in Fig. 7G). However, when *Ift88* was conditionally inactivated in the *SmoM2* ca mutants (*SmoM2/Ift88* cko), the *Shh* and *Foxa2* expression domain was restricted to the ventral midbrain, and *Wnt1* and *Lmx1a* expression were confined to the medial ventral midbrain (Fig. 9C,E,G,I). *Gli1* expression could not be detected in the midbrain of double conditional mutants (Fig. 9A). Moreover, the scattered *Foxa2* expression in the lateral aspects of the *Foxa2* positive domain in *SmoM2/Ift88* cko embryos resembled the phenotype observed in *Ift88* cko mutants (Fig. 9E, compare to control in

Fig. 7D and *Ift88* cko in Fig. 7E) and the size of the Foxa2-positive and the Lmx1a-positive domain in *SmoM2/Ift88* cko mutants was similar to the size of the progenitor domain in *Ift88* cko mutants (Fig. 9Q,R, Fig. 7P,Q). At E12.5, Foxa2 was still expressed throughout most of the dorsal-lateral extent of the midbrain in *SmoM2* ca mutants (Fig. 9L). TH- and Lmx1a-positive mDA neurons were abnormally distributed in *SmoM2* ca mutants (Fig. 9N,P, compare to E13.5 control in Fig. 8*A*). In contrast, the *Foxa2* (Fig. 9K), *Lmx1a* (Fig. 9M) or TH-positive (Fig. 9O) cells were restricted to their normal ventral domains in the *SmoM2/Ift88* cko mutants (compare to E13.5 control in Fig. 8A,C and *Ift88* cko in Fig. 8B,D) (Blaess et al., 2011). These data strongly suggest that the loss of cilia in *Ift88* cko mutants does indeed abolish all Shh signaling downstream of Smo.

4. Discussion

4.1. Primary cilia, Shh signaling, and neurogenesis

In the developing neural tube, Shh is expressed at the floor plate and is responsible for the induction of several neuronal subtypes in a proper ventral to dorsal fashion (Briscoe and Ericson, 2001). In the spinal cord, a wide variety of mouse mutants in proteins involved in ciliary function have been shown to disrupt normal patterning, including Ift88 (Huangfu et al., 2003), Dync2h1 (Huangfu and Anderson, 2005), Ift172 (Huangfu et al., 2003), Ift52 (Liu et al., 2005), Ift57 (Houde et al., 2005), Ift144 (Liem et al., 2012), Ift25 (Keady et al., 2012), and Ftm (Vierkotten et al., 2007). These mutants showed not only a loss of floor plate markers but also a loss of ventrally-located neuronal subtypes such as V3 interneurons and motor neurons. Many of these mutants demonstrated low to no levels of Shh floor plate expression, and all of these demonstrated a loss of Shh signaling, as indicated by both defects in neuronal determination as well as reductions in expression of Shh downstream targets such as *Ptch1* and *Gli1*. We observed a similar outcome in the ventral midbrain of *Ift88* cko mutants, in that Shh and its downstream targets are downregulated shortly after *Ift88* is inactivated, and that a leading neuronal population generated at the ventral VZ, the mDA neuronal population, is severely reduced. We attribute this to the loss of primary cilia in the midbrain of the *Ift88* cko mutants, which begins already at E9.5 and is complete by E10.5. A comparison with spinal cord is interesting in that the *Ift88* mutants display phenotypes very similar to *Gli2*/*Gli3* double mutants (Lei et al., 2004; Motoyama et al., 2003). In our investigation, comparison of floor plate markers and mDA neurogenesis between *Gli2*/*Gli3* cko and *Ift88* cko phenotypes revealed similar defects, including an essentially identical loss in the number of mDA neurons. Given that recombination in both systems is occurring between E8.5 and E9.0, our data indicate the need for mDA progenitors to elaborate functional cilia only before E9.5 in order to allow for specification of mDA neurons. This does not, of course, preclude a later role for primary cilia in the functional maturation of mDA neurons.

Comparison of results obtained with the *cbbs* and *Ift88* cko mutants is particularly instructive. Hypomorphic *cbbs* mutants show a major disorganization in the mDA progenitor domain including rosette-like structures and a loss of clear separation between VZ and mantle layer. Since the ventral midbrain in *Ift88* cko embryos is properly organized, these data suggest that Ift88 might be required for establishing integrity of the neuroepithelium, but only before E8.5. Indeed, examination of the telencephalon and diencephalon of *cbbs* mutants reveals similar rosette-shaped structures and general tissue disorganization (Willaredt et al., 2008). These data indicate that structural integrity of the ventral midbrain progenitor domain might be an important factor in the induction of mDA neuronal fate. Alternatively, *in situ* and qPCR analysis of *Wnt1* expression reveals a downregulation in a factor that is necessary for *Lmx1a* induction. This could explain the more severe phenotype seen in the *cbbs* mutants compared to the *Ift88* cko mice. In addition, our findings are consistent with observations made with the *cbbs* mutants in developing forebrain (Willaredt et al., 2008) and heart (Willaredt et al., 2012). In these organ systems, primary cilia elaborated in the *cbbs* mutants appear morphologically normal, but their transduction of Shh signaling is clearly aberrant, as indicated by reduced *Gli1* expression levels, changes in the proteolytic processing of Gli3 protein, and the morphogenetic abnormalities associated with the respective phenotypes. This apparent contradiction can be explained by the notion that IFT proteins are critical for proper transport of signaling molecules within the Shh pathway, and that a compromise of ciliary signaling function can be detected well before the physical loss of cilia.

Our results are consistent with findings made in the examination of other neuronal populations known to be Shh-dependent. In developing cerebellum, Shh signaling is critical for the expansion, but not the determination, of the progenitor pool giving rise to cerebellar granule cells (Corrales et al., 2006, 2004; Lewis et al., 2004). Conditional deletion of either *Ift88* or *Kif3a* results in a loss of cerebellar granule neurons and a severe hypofoliation of the cerebellum (Chizhikov et al., 2007; Spassky et al., 2008). Interestingly, examination of a conditional mutant in *Smo* revealed an even stronger hypofoliation phenotype (Spassky et al., 2008). Construction of a *Smo*;*Kif3a* double mutant resulted in a phenotype closer in appearance to the *Kif3a* single mutant, indicating that *Kif3a* is epistatic to *Smo* and thus lies downstream of the receptor, just as we have observed in the *SmoM2/Ift88* cko double mutants.

Shh signaling is also crucial for the proliferation and maintenance of adult neural stem cells in the subgranular zone of the postnatal dentate gyrus (Lai et al., 2003; Machold et al., 2003). Mutants in proteins localized to primary cilia such as *Ift88*, *Kif3a*, *Ftm*, and *Stumpy* were shown to be responsible for regulation of hippocampal neurogenesis (Breunig et al., 2008; Han et al., 2008). Conditional ablation of either *Kif3a* or *Smo* in neural progenitors of postnatal hippocampus resulted in a hypoproliferation of progenitors and a failure of neurogenesis (Han et al., 2008). This correlated with a loss of primary cilia in progenitors in the *Kif3a* mutant. As in our study, the authors were unable to rescue neurogenesis in the *Kif3a* mutant background by crossing in an inducible $R26^{SmoM2}$ allele, despite the fact that expression of the $R26^{SmoM2}$ allele in a wild-type background resulted in hyperplasia of the dentate gyrus, as we also saw when $R26^{SmoM2}$ is expressed in the embryonic midbrain. These and our results indicate that both wild-type and the mutant Smo proteins are fundamentally dependent upon primary cilia for their biological function.

4.2. Primary cilia and midbrain development

Cilia serve as signaling hubs integrating information from various pathways including Shh, Wnts, and Fgfs (Goetz and Anderson, 2010). Since members of all these protein families have been implicated in the formation of mDA neurons, it would be conceivable that their effects are mediated by primary cilia. Early (E8.0 – 9.5) Shh signaling plays a critical role in the induction and expansion of mDA progenitors (Blaess et al., 2006, Kabanova et al., 2015). Both Fgf and Wnt signaling regulate subsequent mDA progenitor proliferation and neurogenesis, and conditional inactivation of Wnt or Fgf signaling interferes strongly with the generation or maintenance of mature mDA neurons (Andersson et al., 2013; Fernando et al., 2014; Joksimovic et al., 2009; Lahti et al., 2012; 2011; Tang et al., 2009; 2010; Yang et al., 2013). The fact that mature mDA neurons are generated in *Ift88* cko mutants suggests that cilia are not essential for mediating Wnt or Fgf signaling in mDA neuronal progenitors after E8.5. However, the reductions in the expression levels of *Wnt* growth factors and *Axin2* in *Ift88* cko mutants are likely a direct consequence of the loss of primary cilia, rather than

an indirect effect of the reduction in Shh signaling, since it has been reported that Shh signaling regulates *Wnt1* expression negatively (Hayes et al., 2013; Tang et al., 2013). Moreover, we did not observe an obvious reduction in *Wnt1* expression in the *Gli2/3* cko mutants. In any case, the observed reductions in Wnt expression are not high enough to replicate the documented effects seen when Wnt signaling is genetically ablated in the murine midbrain (Yang et al., 2013). These data, together with the phenotypic similarities of *Ift88* cko and Shh signaling mutants, suggest that the relevance of primary cilia for the genesis of mDA neurons after E8.5 is solely to mediate Shh signaling, and not to integrate other signaling pathways.

Examination of patients with ciliopathies has revealed defects in midbrain-localized structures, such as a failure of the superior cerebellar peduncles to decussate in patients with Joubert syndrome (Poretti et al., 2011). A recent report also listed ill-defined abnormalities in the substantia nigra in two *post-mortem* Joubert syndrome patients (Juric-Sekhar et al., 2012), but whether this reflects a defect in dopaminergic neurogenesis remains to be investigated. In mouse mutants modeling ciliopathies, midbrain defects have only been summarily described. For example, in a mouse mutant for a gene encoding the orphan receptor meckelin (*Tmem67*), which is defective in patients with either Joubert or Meckel syndrome (Baala et al., 2006; Smith et al., 2006) the authors observed a reduction in the length of the rostral–caudal axis of the midbrain tegmentum and occasional midbrain exencephaly (Abdelhamed et al., 2013). Deletion of the gene encoding the IFTA protein Ift172 resulted in a defective midbrain-hindbrain boundary, which formed correctly initially, but lost coherence later (Gorivodsky et al., 2009). However, direct evidence for a dysregulation of mDA development or function caused by ciliopathies or by mutations in ciliary proteins was missing. Our work is the first to demonstrate a role of ciliary proteins in the development of mDA neurons.

5. Conclusions

Our results are consistent with a model in which Shh-dependent induction of mDA neuronal progenitors is critically dependent upon functional primary cilia. We further establish an epistatic relationship in which Smo activity lies upstream of and is dependent upon primary cilia function to carry out its biological effects. In addition, our data suggest that primary cilia are not necessary for events in mDA neurogenesis that are dependent upon Wnt and Fgf signaling. It will be of great interest to conduct more detailed analysis of patients with Joubert or Meckel syndrome, to elucidate if they suffer defects in the generation or function of mDA neurons.

Acknowledgments

The authors were supported by the German Research Society (KLT: DFG SFB 488, Teilprojekt B9; MT: fellowship of the SFB 1049), the University of New England (KLT), the North-Rhine-Westphalia Repatriation Program of the Ministry for Innovation, Science and Research of North Rhine Westphalia (SB); the Maria von Linden-Program, University of Bonn (SB), and the Israeli Science Foundation (CB: grant 1391/11). These funding bodies did not play any role in the design, acquisition, analysis, or interpretation of data, nor did they play a role in drafting the manuscript or revising it critically for intellectual content. The authors would like to thank Joachim Kirsch, Oliver Brüstle, and Thomas Huser for generous scientific support, Marten Smidt for the Aadc and Vmat2 *in situ* probes, Bradley K. Yoder for the *Ift88* floxed line, Andrew McMahon for the $R26^{SmoM2}$ line and Tamara Caspary for the anti-Arl13b antibody. The authors declare no competing financial interests or other conflicts of interest.

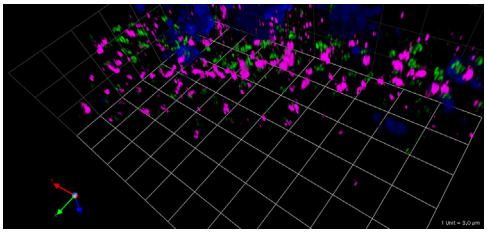

Movie 1. A 3-dimensional reconstruction of an image stack of Fig. 2A recorded by 3D SIM in super-resolution is shown rotating through 360 degrees. A video clip is available online.Supplementary material related to this article can be found online at http://dx.doi.org/10.1016/j.ydbio.2015.10.033.

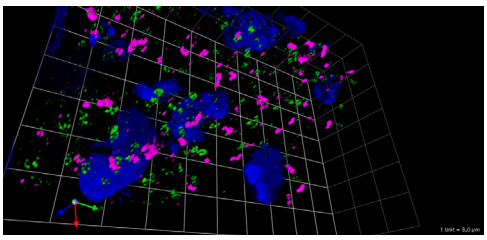

Movie 2. A 3-dimensional reconstruction of an image stack of Fig. 2B recorded by 3D SIM in super-resolution is shown rotating through 360 degrees. A video clip is available online.Supplementary material related to this article can be found online at http://dx.doi.org/10.1016/j.ydbio.2015.10.033.

Appendix A. Supplementary material

Supplementary data associated with this article can be found in the online version at http://dx.doi.org/10.1016/j.ydbio.2015.10.033.

References

Abdelhamed, Z.A., Wheway, G., Szymanska, K., Natarajan, S., Toomes, C., Inglehearn, C., Johnson, C.A., 2013. Variable expressivity of ciliopathy neurological phenotypes that encompass Meckel-Gruber syndrome and Joubert syndrome is caused by complex de-regulated ciliogenesis, Shh and Wnt signalling defects. Hum. Mol. Genet. 22, 1358–1372. http://dx.doi.org/10.1093/hmg/dds546.

Albin, R.L., Young, A.B., Penney, J.B., 1989. The functional-anatomy of basal ganglia disorders. Trends Neurosci. 12, 366–375.

Andersson, E., Tryggvason, U., Deng, Q., Friling, S., Alekseenko, Z., Robert, B., Perlmann, T., Ericson, J., 2006. Identification of intrinsic determinants of midbrain dopamine neurons. Cell 124, 393–405. http://dx.doi.org/10.1016/j.cell.2005.10.037.

Andersson, E.R., Saltó, C., Villaescusa, J.C., Cajanek, L., Yang, S., Bryjova, L., Nagy, I.I., Vainio, S.J., Ramirez, C., Bryja, V., 2013. Wnt5a cooperates with canonical Wnts to generate midbrain dopaminergic neurons in vivo and in stem cells. Proc. Natl. Acad. Sci. USA 110, E602–E610. http://dx.doi.org/10.1073/pnas.1208524110/-/DCSupplemental.

Baala, L., Romano, S., Khaddour, R., Saunier, S., Smith, U.M., Audollent, S., Ozilou, C., Faivre, L., Laurent, N., Foliguet, B., Munnich, A., Lyonnet, S., Salomon, R., Encha-Razavi, F., Gubler, M.-C., Boddaert, N., de Lonlay, P., Johnson, C.A., Vekemans, M., Antignac, C., Attié-Bitach, T., 2006. The Meckel-Gruber syndrome gene, MKS3, is mutated in Joubert syndrome. Am. J. Hum. Genet. 80, 186–194. http://dx.doi.org/10.1086/510499.

Bai, C.B., Stephen, D., Joyner, A.L., 2004. All mouse ventral spinal cord patterning by hedgehog is Gli dependent and involves an activator function of Gli3. Dev. Cell. 6, 103–115.

Bayer, S.A., Wills, K.V., Triarhou, L.C., Ghetti, B., 1995. Time of neuron origin and gradients of neurogenesis in midbrain dopaminergic neurons in the mouse. Exp. Brain Res. 105, 191–199.

Blaess, S., Ang, S.-L., 2015. Genetic control of midbrain dopaminergic neuron development. Wiley Interdiscip. Rev. Dev. Biol. 4, 113–134. http://dx.doi.org/10.1002/wdev.169.

Blaess, S., Bodea, G.O., Kabanova, A., Chanet, S., Mugniery, E., Derouiche, A., Stephen, D., Joyner, A.L., 2011. Temporal-spatial changes in Sonic Hedgehog expression and signaling reveal different potentials of ventral mesencephalic progenitors to populate distinct ventral midbrain nuclei. Neural Dev. 6, 29. http://dx.doi.org/10.1186/1749-8104-6-29.

Blaess, S., Corrales, J.D., Joyner, A.L., 2006. Sonic hedgehog regulates Gli activator and repressor functions with spatial and temporal precision in the mid/hindbrain region. Development 133, 1799–1809. http://dx.doi.org/10.1242/dev.02339.
Blaess, S., Stephen, D., Joyner, A.L., 2008. Gli3 coordinates three-dimensional patterning and growth of the tectum and cerebellum by integrating Shh and Fgf8 signaling. Development 135, 2093–2103. http://dx.doi.org/10.1242/dev.015990.
Bonilla, S., Hall, A.C., Pinto, L., Attardo, A., Götz, M., Huttner, W.B., Arenas, E., 2008. Identification of midbrain floor plate radial glia-like cells as dopaminergic progenitors. Glia 56, 809–820. http://dx.doi.org/10.1002/glia.20654.
Brachmann, I., Jakubick, V.C., Shakèd, M., Unsicker, K., Tucker, K.L., 2007. A simple slice culture system for the imaging of nerve development in embryonic mouse. Dev. Dyn. 236, 3514–3523. http://dx.doi.org/10.1002/dvdy.21386.
Breunig, J., Sarkisian, M., Arellano, J., Morozov, Y., Ayoub, A., Sojitra, S., Wang, B., Flavell, R., Rakic, P., Town, T., 2008. Primary cilia regulate hippocampal neurogenesis by mediating sonic hedgehog signaling. Proc. Natl. Acad. Sci. USA. 105, 13127–13132. http://dx.doi.org/10.1073/pnas.0804558105.
Briscoe, J., Ericson, J., 2001. Specification of neuronal fates in the ventral neural tube. Curr. Opin. Neurobiol. 11, 43–49.
Brodski C., Weissenhorn D.M., Signore M., Sillaber I., Oesterheld M., Broccoli V., Acampora D., Simeone A., and Wurst W., Location and size of dopaminergic and serotonergic cell populations are controlled by the position of the midbrain-hindbrain organizer, J. Neurosci. 23, 2003, 4199-4207.
Caspary, T., Larkins, C.E., Anderson, K.V., 2007. The graded response to Sonic Hedgehog depends on cilia architecture. Dev. Cell. 12, 767–778. http://dx.doi.org/10.1016/j.devcel.2007.03.004.
Chizhikov, V.V., Davenport, J., Zhang, Q., Shih, E.K., Cabello, O.A., Fuchs, J.L., Yoder, B. K., Millen, K.J., 2007. Cilia proteins control cerebellar morphogenesis by promoting expansion of the granule progenitor pool. J. Neurosci. 27, 9780–9789. http://dx.doi.org/10.1523/JNEUROSCI.5586-06.2007.
Corbit, K.C., Aanstad, P., Singla, V., Norman, A.R., Stainier, D.Y.R., Reiter, J.F., 2005. Vertebrate Smoothened functions at the primary cilium. Nature 437, 1018–1021. http://dx.doi.org/10.1038/nature04117.
Corrales, J.D., Blaess, S., Mahoney, E.M., Joyner, A.L., 2006. The level of sonic hedgehog signaling regulates the complexity of cerebellar foliation. Development 133, 1811–1821. http://dx.doi.org/10.1242/dev.02351.
Corrales, J.D., Rocco, G.L., Blaess, S., Guo, Q., Joyner, A.L., 2004. Spatial pattern of sonic hedgehog signaling through Gli genes during cerebellum development. Development 131, 5581–5590. http://dx.doi.org/10.1242/dev.01438.
Deng, Q., Andersson, E., Hedlund, E., Alekseenko, Z., Coppola, E., Panman, L., Millonig, J.H., Brunet, J.-F., Ericson, J., Perlmann, T., 2011. Specific and integrated roles of Lmx1a, Lmx1b and Phox2a in ventral midbrain development. Development 138, 3399–3408. http://dx.doi.org/10.1242/dev.065482.
Farkas, L.M., Dünker, N., Roussa, E., Unsicker, K., Krieglstein, K., 2003. Transforming growth factor-beta(s) are essential for the development of midbrain dopaminergic neurons in vitro and in vivo. J. Neurosci. 23, 5178–5186.
Fernando, C.V., Kele, J., Bye, C.R., Niclis, J.C., Alsanie, W., Blakely, B.D., Stenman, J., Turner, B.J., Parish, C.L., 2014. Diverse roles for Wnt7a in Ventral midbrain neurogenesis and dopaminergic axon morphogenesis. Stem Cells Dev. 23, 1991–2003. http://dx.doi.org/10.1089/scd.2014.0166.
Fuccillo, M., Joyner, A.L., Fishell, G., 2006. Morphogen to mitogen: the multiple roles of hedgehog signalling in vertebrate neural development. Nat. Rev. Neurosci. 7, 772–783. http://dx.doi.org/10.1038/nrn1990.
Goetz, S.C., Anderson, K.V., 2010. The primary cilium: a signalling centre during vertebrate development. Nat. Rev. Genet. 11, 331–344. http://dx.doi.org/10.1038/nrg2774.
Gorivodsky, M., Mukhopadhyay, M., Wilsch-Braeuninger, M., Phillips, M., Teufel, A., Kim, C., Malik, N., Huttner, W., Westphal, H., 2009. Intraflagellar transport protein 172 is essential for primary cilia formation and plays a vital role in patterning the mammalian brain. Dev. Biol. 325, 24–32. http://dx.doi.org/10.1016/j.ydbio.2008.09.019.
Han, Y.-G., Spassky, N., Romaguera-Ros, M., Garcia-Verdugo, J.-M., Aguilar, A., Schneider-Maunoury, S., Alvarez-Buylla, A., 2008. Hedgehog signaling and primary cilia are required for the formation of adult neural stem cells. Nat. Neurosci. 11, 277–284. http://dx.doi.org/10.1038/nn2059.
Haycraft, C.J., Banizs, B., Aydin-Son, Y., Zhang, Q., Michaud, E.J., Yoder, B.K., 2005. Gli2 and Gli3 localize to Cilia and require the intraflagellar transport protein polaris for processing and function. PLoS Genet. 1, e53. http://dx.doi.org/10.1371/journal.pgen.0010053.
Haycraft, C.J., Zhang, Q., Song, B., Jackson, W.S., Detloff, P.J., Serra, R., Yoder, B.K., 2007. Intraflagellar transport is essential for endochondral bone formation. Development 134, 307–316. http://dx.doi.org/10.1242/dev.02732.
Hayes, L., Ralls, S., Wang, H., Ahn, S., 2013. Duration of Shh signaling contributes to mDA neuron diversity. Dev. Biol. 374, 115–126. http://dx.doi.org/10.1016/j.ydbio.2012.11.016.
Houde, C., Dickinson, R.J., Houtzager, V.M., Cullum, R., Montpetit, R., Metzler, M., Simpson, E.M., Roy, S., Hayden, M.R., Hoodless, P.A., Nicholson, D.W., 2005. Hippi is essential for node cilia assembly and Sonic hedgehog signaling. Dev. Biol. 300, 523–533. http://dx.doi.org/10.1016/j.ydbio.2006.09.001.
Hoyer-Fender S., Primary and motile cilia: their ultrastructure and ciliogenesis In: Tucker, K.L. and Caspary, T (Eds). Cilia and Nervous System Development and Function Springer, Germany pp. 1-53.
Huang, P., Schier, A.F., 2009. Dampened Hedgehog signaling but normal Wnt signaling in zebrafish without cilia. Development 136, 3089–3098. http://dx.doi.org/10.1242/dev.041343.
Huangfu, D., Anderson, K.V., 2005. Cilia and Hedgehog responsiveness in the mouse. Proc. Natl. Acad. Sci. USA 102, 11325–11330. http://dx.doi.org/10.1073/pnas.0505328102.
Huangfu, D., Liu, A., Rakeman, A.S., Murcia, N.S., Niswander, L., Anderson, K.V., 2003. Hedgehog signalling in the mouse requires intraflagellar transport proteins. Nature, 83–87.
Hui, C.C., Joyner, A.L., 1993. A mouse model of greig cephalopolysyndactyly syndrome: the extra-toesJ mutation contains an intragenic deletion of the Gli3 gene. Nat. Genet. 3, 241–246. http://dx.doi.org/10.1038/ng0393-241.
Jeong, J., Mao, J., Tenzen, T., Kottmann, A.H., McMahon, A.P., 2004. Hedgehog signaling in the neural crest cells regulates the patterning and growth of facial primordia. Genes. Dev. 18, 937–951.
Jho, E.-H., Zhang, T., Domon, C., Joo, C.-K., Freund, J.-N., Costantini, F., 2002. Wnt/beta-catenin/Tcf signaling induces the transcription of Axin2, a negative regulator of the signaling pathway. Mol. Cell. Biol. 22, 1172–1183.
Joksimovic, M., Yun, B.A., Kittappa, R., Anderegg, A.M., Chang, W.W., Taketo, M.M., McKay, R.D.G., Awatramani, R.B., 2009. Wnt antagonism of Shh facilitates midbrain floor plate neurogenesis. Nat. Neurosci. 12, 125–131. http://dx.doi.org/10.1038/nn.2243.
Juric-Sekhar, G., Adkins, J., Doherty, D., Hevner, R.F., 2012. Joubert syndrome: brain and spinal cord malformations in genotyped cases and implications for neurodevelopmental functions of primary cilia. Acta Neuropathol. 123, 695–709. http://dx.doi.org/10.1007/s00401-012-0951-2.
Kabanova, A., Pabst, M., Lorkowski, M., Braganza, O., Boehlen, A., Nikbakht, N., Pothmann, L., Vaswani, A.R., Musgrove, R., Di Monte, D.A., Sauvage, M., Beck, H., Blaess, S., 2015. Function and developmental origin of a mesocortical inhibitory circuit. Nat. Neurosci. 18; , pp. 872–882. http://dx.doi.org/10.1038/nn.4020.
Kang, W.-Y., Kim, S.-S., Cho, S.-K., Kim, S., Suh-Kim, H., Lee, Y.-D., 2010. Migratory defect of mesencephalic dopaminergic neurons in developing reelermice. Anat. Cell. Biol. 43, 241. http://dx.doi.org/10.5115/acb.2010.43.3.241.
Keady, B.T., Samtani, R., Tobita, K., Tsuchya, M., Agustin, J.T.S., Follit, J.A., Jonassen, J. A., Subramanian, R., Lo, C.W., Pazour, G.J., 2012. IFT25 links the signal-dependent movement of Hedgehog components to Intraflagellar transport. Dev. Cell 22, 940–951. http://dx.doi.org/10.1016/j.devcel.2012.04.009.
Kimmel, R.A., Turnbull, D.H., Blanquet, V., Wurst, W., Loomis, C.A., Joyner, A.L., 2000. Two lineage boundaries coordinate vertebrate apical ectodermal ridge formation. Genes. Dev. 14, 1377–1389.
Lahti, L., Peltopuro, P., Piepponen, T.P., Partanen, J., 2012. Cell-autonomous FGF signaling regulates anteroposterior patterning and neuronal differentiation in the mesodiencephalic dopaminergic progenitor domain. Development 139, 894–905. http://dx.doi.org/10.1242/dev.071936.
Lahti, L., Saarimäki-Vire, J., Rita, H., Partanen, J., 2011. FGF signaling gradient maintains symmetrical proliferative divisions of midbrain neuronal progenitors. Dev. Biol. 349, 270–282. http://dx.doi.org/10.1016/j.ydbio.2010.11.008.
Lai, K., Kaspar, B.K., Gage, F.H., Schaffer, D.V., 2003. Sonic hedgehog regulates adult neural progenitor proliferation in vitro and in vivo. Nat. Neurosci. 6, 21–27. http://dx.doi.org/10.1038/nn983.
Lancaster, M.A., Schroth, J., Gleeson, J.G., 2011. Subcellular spatial regulation of canonical Wnt signalling at the primary cilium. Nat. Cell. Biol. 13, 700–707. http://dx.doi.org/10.1038/ncb2259.
Lei, Q., Zelman, A.K., Kuang, E., Li, S., Matise, M.P., 2004. Transduction of graded Hedgehog signaling by a combination of Gli2 and Gli3 activator functions in the developing spinal cord. Development 131, 3593–3604. http://dx.doi.org/10.1242/dev.01230.
Lewis, P.M., Gritli-Linde, A., Smeyne, R., Kottmann, A., McMahon, A.P., 2004. Sonic hedgehog signaling is required for expansion of granule neuron precursors and patterning of the mouse cerebellum. Dev. Biol. 270, 393–410. http://dx.doi.org/10.1016/j.ydbio.2004.03.007.
Liem, K.F., Ashe, A., He, M., Satir, P., Moran, J., Beier, D., Wicking, C., Anderson, K.V., 2012. The IFT-A complex regulates Shh signaling through cilia structure and membrane protein trafficking. J. Cell. Biol. 197, 789–800. http://dx.doi.org/10.1083/jcb.201110049.
Lienkamp, S., Ganner, A., Walz, G., 2012. Inversin, Wnt signaling and primary cilia. Differentiation 83, S49–S55. http://dx.doi.org/10.1016/j.diff.2011.11.012.
Lin, W., Metzakopian, E., Mavromatakis, Y.E., Gao, N., Balaskas, N., Sasaki, H., Briscoe, J., Whitsett, J.A., Goulding, M., Kaestner, K.H., Ang, S.-L., 2009. Foxa1 and Foxa2 function both upstream of and cooperatively with Lmx1a and Lmx1b in a feedforward loop promoting mesodiencephalic dopaminergic neuron development. Dev. Biol. 333, 386–396. http://dx.doi.org/10.1016/j.ydbio.2009.07.006.
Liu, A., Wang, B., Niswander, L.A., 2005. Mouse intraflagellar transport proteins regulate both the activator and repressor functions of Gli transcription factors. Development 132, 3103–3111. http://dx.doi.org/10.1242/dev.01894.
Machold, R., Hayashi, S., Rutlin, M., Muzumdar, M.D., Nery, S., Corbin, J.G., Gritli-Linde, A., Dellovade, T., Porter, J.A., Rubin, L.L., Dudek, H., McMahon, A.P., Fishell, G., 2003. Sonic hedgehog is required for progenitor cell maintenance in telencephalic stem cell niches. Neuron 39, 937–950.
Matise, M.P., Epstein, D.J., Park, H.L., Platt, K.A., Joyner, A.L., 1998. Gli2 is required for induction of floor plate and adjacent cells, but not most ventral neurons in the mouse central nervous system. Development 125, 2759–2770.
Mavromatakis, Y.E., Lin, W., Metzakopian, E., Ferri, A.L.M., Yan, C.H., Sasaki, H., Whisett, J., Ang, S.-L., 2011. Foxa1 and Foxa2 positively and negatively regulate Shh signalling to specify ventral midbrain progenitor identity. Mech. Dev. 128,

90–103. http://dx.doi.org/10.1016/j.mod.2010.11.002.
Motoyama, J., Milenkovic, L., Iwama, M., Shikata, Y., Scott, M.P., Hui, C.-C., 2003. Differential requirement for Gli2 and Gli3 in ventral neural cell fate specification. Dev. Biol. 259, 150–161.
Nakatani, T., Kumai, M., Mizuhara, E., Minaki, Y., Ono, Y., 2010. Lmx1a and Lmx1b cooperate with Foxa2 to coordinate the specification of dopaminergic neurons and control of floor plate cell differentiation in the developing mesencephalon. Dev. Biol. 339, 101–113. http://dx.doi.org/10.1016/j.ydbio.2009.12.017.
Ocbina, P.J.R., Tuson, M., Anderson, K.V., 2009. Primary cilia are not required for normal canonical Wnt signaling in the mouse embryo. PLoS One 4, e6839. http://dx.doi.org/10.1371/journal.pone.0006839.g004.
Oh, E.C., Katsanis, N., 2012. Context-dependent regulation of Wnt signaling through the primary cilium. J. Am. Soc. Nephrol. 24, 10–18. http://dx.doi.org/10.1681/ASN.2012050526.
Pazour, G.J., 2002. The intraflagellar transport protein, IFT88, is essential for vertebrate photoreceptor assembly and maintenance. J. Cell. Biol. 157, 103–114. http://dx.doi.org/10.1083/jcb.200107108.
Poretti, A.A., Huisman, T.A.G.M.T., Scheer, I.I., Boltshauser, E.E., 2011. Joubert syndrome and related disorders: spectrum of neuroimaging findings in 75 patients. AJNR Am. J. Neuroradiol. 32, 1459–1463. http://dx.doi.org/10.3174/ajnr.A2517.
Prakash, N., Puelles, E., Freude, K., Trümbach, D., Omodei, D., Di Salvio, M., Sussel, L., Ericson, J., Sander, M., Simeone, A., Wurst, W., 2009. Nkx6-1 controls the identity and fate of red nucleus and oculomotor neurons in the mouse midbrain. Development 136, 2545–2555. http://dx.doi.org/10.1242/dev.031781.
Rohatgi, R., Milenkovic, L., Scott, M.P., 2007. Patched1 regulates Hedgehog signaling at the primary Cilium. Science 317, 372–376. http://dx.doi.org/10.1126/science.1139740.
Santos, N., Reiter, J.F., 2014. A central region of Gli2 regulates its localization to the primary cilium and transcriptional activity. J. Cell Sci. 127, 1500–1510. http://dx.doi.org/10.1242/jcs.139253.
Scholey J.M., Intraflagellar Transport, Ann. Rev. Dev. Cell Biol. 19, 2003, 423-443, http://dx.doi.org/10.1146/annurev.cellbio.19.111401.091318.
Smith, U.M., Consugar, M., Tee, L.J., McKee, B.M., Maina, E.N., Whelan, S., Morgan, N. V., Goranson, E., Gissen, P., Lilliquist, S., Aligianis, I.A., Ward, C.J., Pasha, S., Punyashthiti, R., Sharif, S.M., Batman, P.A., Bennett, C.P., Woods, C.G., McKeown, C., Bucourt, M., Miller, C.A., Cox, P., AlGazali, L., Trembath, R.C., Torres, V.E., Attié-Bitach, T., Kelly, D.A., Maher, E.R., Gattone, V.H., Harris, P.C., Johnson, C.A., 2006. The transmembrane protein meckelin (MKS3) is mutated in Meckel-Gruber syndrome and the wpk rat. Nat. Genet. 38, 191–196. http://dx.doi.org/10.1038/ng1713.
Spassky, N., Han, Y.-G., Aguilar, A., Strehl, L., Besse, L., Laclef, C., Ros, M.R., Garcia-Verdugo, J.M., Alvarez-Buylla, A., 2008. Primary cilia are required for cerebellar development and Shh-dependent expansion of progenitor pool. Dev. Biol. 317, 246–259. http://dx.doi.org/10.1016/j.ydbio.2008.02.026.
Tang, M., Luo, S.X., Tang, V., Huang, E.J., 2013. Temporal and spatial requirements of Smoothened in ventral midbrain neuronal development. Neural Dev. 8. http://dx.doi.org/10.1186/1749-8104-8-8 1–1.
Tang, M., Miyamoto, Y., Huang, E.J., 2009. Multiple roles of beta-catenin in controlling the neurogenic niche for midbrain dopamine neurons. Development 136, 2027–2038. http://dx.doi.org/10.1242/dev.034330.
Tang, M., Villaescusa, J.C., Luo, S.X., Guitarte, C., Lei, S., Miyamoto, Y., Taketo, M.M., Arenas, E., Huang, E.J., 2010. Interactions of Wnt/beta-Catenin signaling and sonic Hedgehog Regulate the neurogenesis of ventral midbrain dopamine neurons. J. Neurosci. 30, 9280–9291. http://dx.doi.org/10.1523/JNEUROSCI.0860-10.2010.
Tasouri, E., Tucker, K.L., 2011. Primary cilia and organogenesis: is Hedgehog the only sculptor? Cell Tissue Res. 345, 21–40. http://dx.doi.org/10.1007/s00441-011-1192-8.
Tran, P.V., Haycraft, C.J., Besschetnova, T.Y., Turbe-Doan, A., Stottmann, R.W., Herron, B.J., Chesebro, A.L., Qiu, H., Scherz, P.J., Shah, J.V., Yoder, B.K., Beier, D.R., 2008. THM1 negatively modulates mouse sonic hedgehog signal transduction and affects retrograde intraflagellar transport in cilia. Nat. Genet. 40, 403–410. http://dx.doi.org/10.1038/ng.105.
Tye, K.M., Mirzabekov, J.J., Warden, M.R., Ferenczi, E.A., Tsai, H.-C., Finkelstein, J., Kim, S.-Y., Adhikari, A., Thompson, K.R., Andalman, A.S., Gunaydin, L.A., Witten, I.B., Deisseroth, K., 2013. Dopamine neurons modulate neural encoding and expression of depression-related behaviour. Nature 493, 537–541. http://dx.doi.org/10.1038/nature11740.
Vierkotten, J., Dildrop, R., Peters, T., Wang, B., Rüther, U., 2007. Ftm is a novel basal body protein of cilia involved in Shh signalling. Development 134, 2569–2577. http://dx.doi.org/10.1242/dev.003715.
Willaredt, M.A., Gorgas, K., Gardner, H.A.R., Tucker, K.L., 2012. Multiple essential roles for primary cilia in heart development. Cilia 1, 23. http://dx.doi.org/10.1186/2046-2530-1-23.
Willaredt, M.A., Hasenpusch-Theil, K., Gardner, H.A.R., Kitanovic, I., Hirschfeld-Warneken, V.C., Gojak, C.P., Gorgas, K., Bradford, C.L., Spatz, J., Wölfl, S., Theil, T., Tucker, K.L., 2008. A crucial role for primary cilia in cortical morphogenesis. J. Neurosci. 28, 12887–12900. http://dx.doi.org/10.1523/JNEUROSCI.2084-08.2008.
Winterer, G., Weinberger, D.R., 2004. Genes, dopamine and cortical signal-to-noise ratio in schizophrenia. Trends Neurosci. 27, 683–690. http://dx.doi.org/10.1016/j.tins.2004.08.002.
Yan, C.H., Levesque, M., Claxton, S., Johnson, R.L., Ang, S.-L., 2011. Lmx1a and lmx1b function cooperatively to regulate proliferation, specification, and differentiation of midbrain dopaminergic progenitors. J. Neurosci. 31, 12413–12425. http://dx.doi.org/10.1523/JNEUROSCI.1077-11.2011.
Yang, J., Brown, A., Ellisor, D., Paul, E., Hagan, N., Zervas, M., 2013. Dynamic temporal requirement of Wnt1 in midbrain dopamine neuron development. Development 140, 1342–1352. http://dx.doi.org/10.1242/dev.080630.
Ye, W., Shimamura, K., Rubenstein, J.L., Hynes, M.A., Rosenthal, A., 1998. FGF and Shh signals control dopaminergic and serotonergic cell fate in the anterior neural plate. Cell 93, 755–766.